

## Topical Review

# Pulsed plasma etching for semiconductor manufacturing

Demetre J Economou

Plasma Processing Laboratory, Department of Chemical and Biomolecular Engineering, University of Houston, Houston, TX 77204-4004, USA

E-mail: [Economou@uh.edu](mailto:Economou@uh.edu)

Received 21 January 2014, revised 16 April 2014

Accepted for publication 22 May 2014

Published 1 July 2014

### Abstract

Power-modulated (*pulsed*) plasmas have demonstrated several advantages compared to continuous wave (CW) plasmas. Specifically, pulsed plasmas can result in a higher etching rate, better uniformity, and less structural, electrical or radiation (e.g. vacuum ultraviolet) damage. Pulsed plasmas can also ameliorate unwanted artefacts in etched micro-features such as notching, bowing, micro-trenching and aspect ratio dependent etching. As such, pulsed plasmas may be indispensable in etching of the next generation of micro-devices with a characteristic feature size in the sub-10 nm regime. This work provides an overview of principles and applications of pulsed plasmas in both electropositive (e.g. argon) and electronegative (e.g. chlorine) gases. The effect of pulsing the plasma source power (*source pulsing*), the electrode bias power (*bias pulsing*), or both source and bias power (*synchronous pulsing*), on the time evolution of species densities, electron energy distribution function and ion energy and angular distributions on the substrate is discussed. The resulting pulsed plasma process output (etching rate, uniformity, damage, etc) is compared, whenever possible, to that of CW plasma, under otherwise the same or similar conditions.

Keywords: pulsed plasma, microelectronics, plasma processing

(Some figures may appear in colour only in the online journal)

## 1. Introduction

Low temperature non-equilibrium glow discharge plasmas are a workhorse in the fabrication of microelectronic devices. They are used mainly for etching and deposition of thin films, but also for other unit processes, such as shallow ion implantation [1, 2]. Typical range of conditions under which these plasmas operate are: pressure  $\sim 0.1$  mTorr to 10 Torr, gas temperature  $\sim 300$ – $600$  K and degree of ionization (mole fraction of charged species)  $\sim 10^{-1}$ – $10^{-6}$ . Low temperature plasmas also find extensive use in lighting, surface modification (e.g. to effect corrosion resistance or hardening), even environmental remediation. Furthermore, atmospheric pressure non-equilibrium glow discharges are currently being intensively investigated in connection with the burgeoning field of plasma medicine [3]. Figure 1 is a panorama of plasma etching, taking polysilicon etching with chlorine as

an example. Radio frequency (RF) or microwave power (source power) generates and sustains a plasma in a partially evacuated chamber. In the example of figure 1 the plasma is powered by an RF inductive coil on top of a dielectric window. Feed gas (e.g. chlorine) enters the reactor at a specified flow rate. Spent gas and reaction by-products (e.g.  $\text{SiCl}_4$ ) are evacuated by a pumping system. Energetic plasma electrons dissociate and ionize the feedstock gas to produce Cl radicals and  $\text{Cl}_2^+$  ions (figure 1(a)). Positive ions drift towards the reactor walls and enter the sheath, where they accelerate in the direction perpendicular to the wafer. The sheath (figure 1(b)), a boundary layer naturally forming over any material surface in contact with plasma, is a region of net positive charge resulting in a relatively high electric field. Neutral radical species have no directionality. They are transported by convective gas flow and diffusion, and adsorb on the silicon wafer. Ion bombardment of the silicon wafer

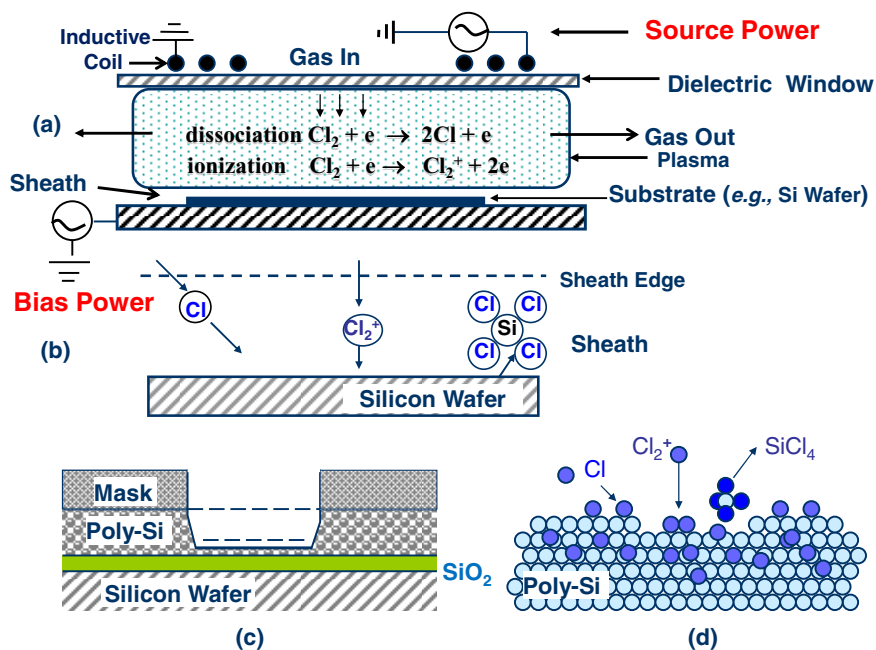


**Figure 1.** Panorama of plasma etching using silicon etching with chlorine as an example. (a) The source power generates plasma, in this case an ICP, which controls the plasma density. The bias power on the substrate electrode controls the energy of ions bombarding the wafer. Cl radicals and  $\text{Cl}_2^+$  ions are generated in the plasma by electron impact on  $\text{Cl}_2$  molecules. (b) Close-up view of the sheath over the wafer. Ions accelerate in the sheath and bombard the wafer along the vertical direction (anisotropically). At the same time isotropic neutrals strike the wafer. The combination of neutral and energetic ion bombardment results in the formation of etch products. (c) Close-up view of an etching micro-feature. Ion bombardment induces anisotropic etching, replicating the mask pattern into the poly-Si film. (d) Close-up view of the silicon lattice. Ion bombardment creates a modified surface layer where Cl is mixed within the Si lattice to a depth of  $\sim 10 \text{ \AA}$ , depending on the ion energy. Activation of this layer by ion bombardment yields etching products that desorb into the gas phase. In the pulsed plasma operation, the source or bias power (or both) are modulated in time.

promotes the formation of reaction products that are either sputtered ( $\text{SiCl}_x$ ,  $x = 1, 2, 3$ ) or desorb spontaneously ( $\text{SiCl}_4$ ) in the gas phase. When ion bombardment is necessary for etching to occur (e.g. p-type silicon), anisotropic etching can be obtained, since etching occurs only at the bottom of the micro-feature (figure 1(c)) where ions strike the surface, provided ions maintain their directionality (for example no collisions in the sheath). If radicals can etch the wafer spontaneously (without the presence of ion bombardment) as, for example, in the case of heavily doped n-type Si, then a sidewall passivation mechanism is necessary to achieve anisotropy. At the atomic level, ions bombarding the wafer with energy of 10s–100s of eV create a cascade of breaking and forming bonds that yields chlorinated silicon reaction products (figure 1(d)). Activation occurs in a modified layer at the top of the solid, the depth of which depends mainly on ion energy. Besides the RF source power, a separate RF power supply (bias power) may be connected to the substrate electrode. The source power is normally at relatively high frequencies (10–100 MHz) and its function is to generate plasma to control the plasma density. The bias power is normally at lower frequencies (100s kHz to 10 MHz) and is used to control the ion bombardment energy. This reactor configuration provides some degree of independent control of ion flux and ion energy on the substrate, in contrast to classical capacitively coupled plasma (CCP) reactors in which ion flux and ion bombardment energy are intimately coupled.

The goals of any plasma etching process are high throughput, high uniformity, high selectivity, anisotropy and

no damage. Throughput (wafers per unit time) is a measure of productivity. Uniformity across the wafer and from wafer-to-wafer is required so that the devices produced are within specifications. Selectivity is required with respect to both the masking layer and the underlying layer (silicon dioxide in figure 1(c)). The mask must not etch or critical dimension (CD) control is difficult to achieve. Selectivity with respect to the underlayer is important when the plasma or the thickness of the film to be etched is not uniform. Such situations necessitate overetching, exposing the underlayer to potentially harmful plasma in places where the film has been etched to end-point, while other areas of the wafer are yet to clear. Anisotropy refers to the shape of the micro-feature wall profile. Almost vertical sidewalls, perhaps with some rounding of the bottom of the feature, is often required. Damage can occur by several mechanisms, including (a) amorphization of the top layers of the substrate by ion bombardment, (b) radiation damage due to UV, VUV and soft x-rays originating in the plasma [4]. In particular, VUV radiation can lead to undesired etching and distorted wall profiles of nanoscale features [5], and (c) charging damage. The latter can in turn be distinguished in charging and breakdown of insulating films (e.g. gate oxides) due to non-uniform plasma [6], or charging damage due to the electron shading effect. Since electrons have high temperature ( $\sim 1\text{--}10 \text{ eV}$ ), are repelled by the sheath, and suffer momentum randomizing collisions, the flux of electrons on the wafer is essentially isotropic. On the contrary, positive ions have low temperature ( $\sim 0.1 \text{ eV}$ ) and are accelerated in the sheath,

perpendicular to the wafer, resulting in a flux on the surface that is highly anisotropic. This difference in flux directionalities can cause a localized build-up of negative charge at the top, mouth entrance, and sidewalls of insulating features, and a positive charge at the bottom of the features. The local electric field established by this differential charging [7, 8] is believed to deflect further oncoming positive ions causing etch profile distortions (notching and/or bowing [9, 10], micro-trenching [11], etc) and aspect ratio dependent etching (ARDE) [12]. In ARDE, the etch rate of micro-features depends on the feature aspect ratio (depth/width) and usually decreases as the aspect ratio increases.

As device dimensions continue to shrink into the sub-10 nm regime, achieving the goals of plasma etching mentioned above becomes extremely challenging. There are many externally controlled variables (process inputs) which can influence the process output (figure 2). Given a reactor type (e.g. CCP, inductively coupled plasma (ICP), electron cyclotron resonance (ECR), plasma, etc), its geometrical configuration and materials of construction, one can manipulate operating parameters (pressure, power, frequency, gas composition, gas flow rate, etc) to influence the process output (etching rate, uniformity, anisotropy, damage, etc). Rational selection of reactor design and plasma chemistry can be facilitated by understanding the fundamentals of the chemical and physical processes taking place in the plasma and on the wafer surface. Such understanding can be obtained by bridging the gap between the process inputs and outputs through key plasma properties (figure 2).

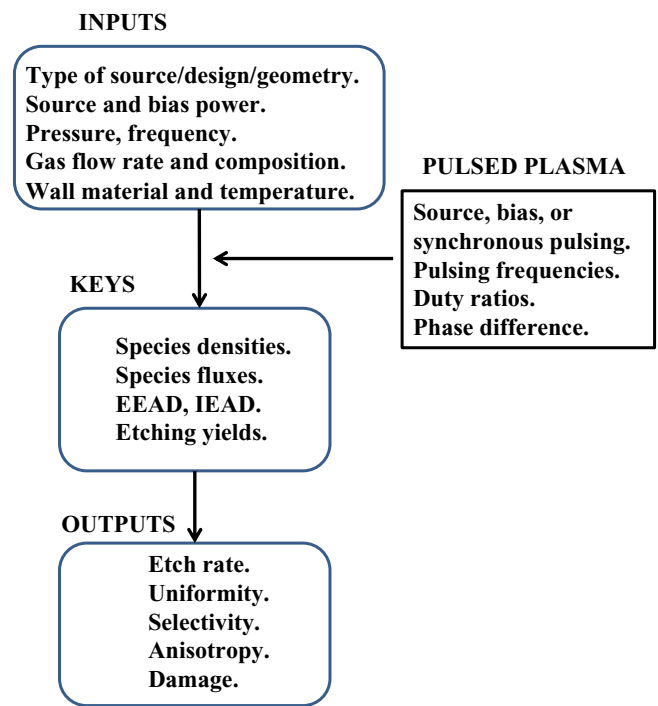


**Figure 2.** The key internal plasma properties bridge the gap between the plasma etch process inputs (control variables) and outputs. Pulsing the plasma adds more ‘knobs’ (type of pulsing, pulsing frequencies, duty ratios) to a plethora of inputs (EEAD = electron energy and angular distribution, IEAD = ion energy and angular distribution).

## 2. Pulsed plasmas

Pulsed plasmas have emerged as promising candidates to address the formidable challenges of fabricating future generations of micro-devices. This is especially the case for electronegative gas plasmas (e.g. Cl<sub>2</sub>, HBr, SF<sub>6</sub>, O<sub>2</sub>, fluorocarbons, etc) which are used extensively in industrial practice. Experiments using pulsed electronegative discharges have shown suppression of anomalous etch profiles (e.g. notching) during poly-Si etching, and reduced charging damage of the gate insulator [13–16]. This improvement in the etching characteristics of pulsed electronegative discharges, compared to conventional continuous wave (CW) operation, has been attributed (at least in part) to negative ions. More recent studies have shown reduced damage to the Si substrate during gate etching [17]. Furthermore, pulsed plasmas offer other important advantages (compared to CW plasmas) including (a) improved etch selectivity by, for example, modifying the concentration of chemical species present in the plasma [18–20], (b) improved etch or deposition rate [21, 22], (c) reduced dust generation [23–26] and (d) improved etch or deposition uniformity [22, 27, 28]. A review of pulsed plasmas, focusing on high density reactors, has been presented by Banna *et al* [29].

In pulsed plasmas the power fed to the reactor is modulated in time. Square wave modulation is most frequently applied as shown in figure 3. The duration of the power ON fraction of the cycle (active glow) is  $\tau_{ON}$ , while that of the power

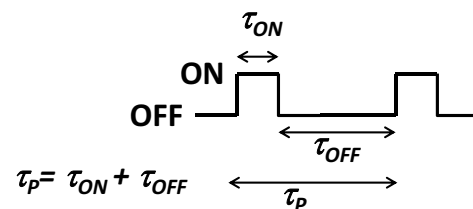


**Figure 3.** In pulsed plasmas, power is square-wave modulated. Within each pulse, the power is ON for time  $\tau_{ON}$  and OFF for time  $\tau_{OFF}$ . The pulse period is  $\tau_P = \tau_{ON} + \tau_{OFF}$  and the duty ratio is  $D = \tau_{ON}/\tau_P$ . The pulsing frequency is usually 10 kHz or lower. During power ON, the plasma excitation frequency is usually from RF to microwave.

OFF fraction of the cycle (afterglow) is  $\tau_{OFF}$ . The pulse period is  $\tau_P = \tau_{ON} + \tau_{OFF}$ , and the duty ratio (or duty cycle) is defined as  $D = \tau_{ON}/\tau_P$ , i.e. the fraction of the cycle with power ON. Usually 100% power modulation depth is applied, i.e. the power in the afterglow is zero. Partial power modulation has also been used, for the purpose of measuring the kinetics of plasma-chemical or wall reactions [30, 31], and will not be considered here. The following cases of power modulation may be encountered (figure 4): (a) modulation of the power that sustains the plasma (*source pulsing*) with no power on the substrate electrode, (b) modulation of the power that sustains the plasma (*source pulsing*) with CW power on the substrate electrode, (c) modulation of the power to the substrate electrode (*bias pulsing*) with CW source power, and (d) modulation of both the source and bias powers with or without a phase shift between the two (*synchronous pulsing*).

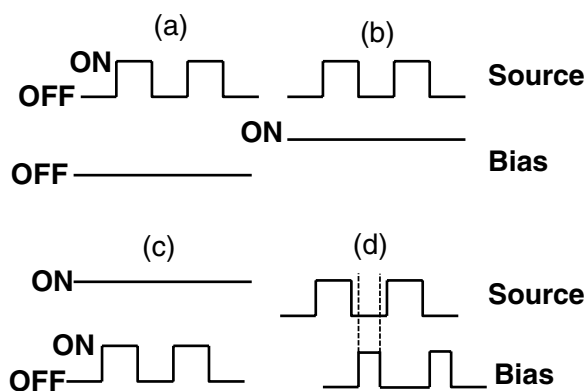


**Figure 4.** Common pulsed plasma schemes. (a) Source pulsing with no substrate bias. (b) Source pulsing with CW substrate bias. (c) Bias pulsing with CW source power. (d) Synchronous source and bias pulsing, where bias power may be phase shifted with respect to the source power. In synchronous pulsing, the PRF is the same for both source and bias, but the duty ratios can differ. The pulsing frequency is usually 10 kHz or lower. The plasma source is usually powered with frequencies from RF to microwave. Electrode bias is usually RF or dc.

Synchronous in this context means that both the source and bias powers are modulated with the same frequency, but the duty ratios can be different. The source power is usually at frequencies from RF to microwave. Bias power is usually RF or dc. One more configuration (not shown in figure 4) that will be discussed involves source pulsing with synchronous bias on an auxiliary electrode (so-called *boundary electrode* (BE)) that controls the plasma potential [32–34]. In this case, the substrate electrode may be grounded or biased with an independent power supply.

It should be noted that power turn ON or OFF is often assumed instantaneous. In practice, there is a ‘ramp-up’ and a ‘ramp-down’ time which can make a difference in heating of the electron energy distribution function (EEDF). Based on the findings of Lafleur and Booth [35], for example, the faster the rate of change of the applied voltage, the more the heating of the EEDF. When the plasma is pulsed, in addition to the type of pulsing (source, bias or synchronous) there are at least two new input variables, namely, pulse period (or its equivalent, pulse repetition frequency (PRF)) and duty ratio. The addition of more variables to the plethora of the already existing ones (figure 2) makes plasma reactor or process optimization a daunting task. On the other hand, additional ‘knobs’ increase process flexibility.

### 3. Time evolution of pulsed electronegative plasmas (figures 5–7)

Industrial plasma processes employ electronegative gases. For example, etching of silicon, silicon dioxide or polymers is carried out with halogen-containing gases, fluorocarbons or oxygen-containing plasmas, respectively [1, 2]. Electronegative gas plasmas tend to stratify: negative ions pile-up in the central region of the plasma forming an electronegative core, surrounded by a region devoid of negative ions (electropositive periphery), followed by the

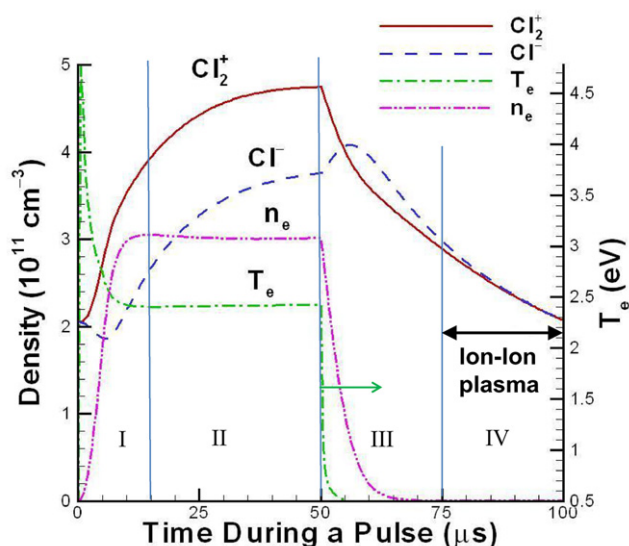


**Figure 5.** Time evolution of species densities (left axis) and electron temperature (right axis) predicted by a pulsed plasma model in chlorine. Plasma source was pulsed with a period of 100 μs and duty ratio = 50%. There was no substrate bias. Peak power = 320 W, pressure = 20 mTorr. Each pulse is separated in four time windows: early active glow (I), late active glow (II), early afterglow (III) and late afterglow (IV). Only the major ion Cl<sub>2</sub><sup>+</sup> density is shown (Cl<sup>+</sup> is not included). From [76] with permission. Copyright 2002 American Vacuum Society.

wall sheath which contains only positive ions and electrons. For high enough negative-ion densities, the electropositive periphery is squeezed, and eventually the negative ions reach the sheath edge. Negative ions cannot enter the sheath since the negative-ion energy is far less than the sheath potential. The stratification of electronegative discharges has been studied extensively, particularly for collisional plasmas [1, 36–39]. Abrupt transitions and oscillatory behaviour of the potential in the plasma have also been reported [40–42]. In CW plasmas, negative ions are trapped in the plasma by the electrostatic field. Therefore negative ions cannot reach the substrate. Pulsing the plasma (source pulsing) provides a means to having a negative-ion flux bombarding the substrate. This is because in the afterglow of the pulsed plasma, the electrostatic field disintegrates, allowing negative ions to diffuse from the plasma core to the wall. Combining source pulsing with low frequency RF substrate bias can result in alternating acceleration of positive and negative ions out of the plasma and onto the wafer. Such action can reduce charging damage, and improve etch results [13, 14, 43, 44]. It was suggested that, because positive and negative ions have comparable masses and similar velocity anisotropy under acceleration by low frequency sinusoidal bias, differential charging [7, 8] of the walls of micro-features was reduced ameliorating charging damage.

Midha and Economou [45] reported a model of a pulsed ICP (source pulsing, no substrate bias) under the following conditions: power density 1 W cm<sup>-3</sup>, pressure 20 mTorr, interelectrode spacing 3.8 cm, pulse period 100 μs and duty ratio 50%. Figure 5 shows the time evolution of species densities (left y-axis) and electron temperature (right y-axis) at the *central plane* of the reactor, after reaching a periodic

steady-state. The source power was turned ON at  $t = 0 \mu\text{s}$  and OFF at  $t = 50 \mu\text{s}$ . The trends shown in figure 5 are in good agreement with experimental results reported in the literature [46–48]. The power ON fraction of the cycle (active glow,  $t = 0 - 50 \mu\text{s}$ ) is separated into early active glow (region I in figure 5) and late active glow (region II). The power OFF fraction of the cycle (afterglow,  $t = 50 - 100 \mu\text{s}$ ) is separated into early afterglow (region III) and late afterglow (region IV). The electron temperature goes through a sharp maximum at the very early active glow and settles to a quasi-steady value within  $\sim 10 \mu\text{s}$  into the pulse. In the afterglow,  $T_e$  plummets to 0.5 eV within  $\sim 5 \mu\text{s}$  after power is turned OFF. The electron density is severely modulated during a cycle. It increases monotonically after the power is turned ON, only to reach a quasi-steady value by the end of the early active glow. The electron density decays in the afterglow reaching very low values by the end of the early afterglow. In contrast, the positive- and negative-ion densities are much less modulated. The positive-ion density increases in the active glow and decreases in the afterglow. The negative-ion density goes through a shallow minimum in the early active glow and then keeps on increasing for the remainder of the active glow. Upon power turn OFF, the negative-ion density goes through a small peak in the early afterglow and then decreases for the remainder of the afterglow. The plasma is weakly electronegative (ratio of electron to negative-ion density  $\sim 1$ ) in the active glow and then becomes progressively more electronegative in the afterglow. The electron density decays rapidly in the afterglow, eventually becoming negligible compared to the negative-ion density. At that point a positive-ion negative-ion (ion–ion) plasma forms [49]. In an ion–ion plasma, the ambipolar field can be approximated by [45, 50],

$$E \approx \left[ \frac{(D_p - D_n)\nabla n_n}{(\mu_n + \mu_p)n_n} \right]. \quad (1)$$

This field is much reduced compared to that in an electropositive discharge  $E = -T_e(\nabla n_e/n_e)$ . The negative ions essentially neutralize the space charge field. Here  $D$  is the (free) species diffusivity, and  $n$  and  $\mu$  are species density and mobility, respectively. Subscripts  $p$ ,  $n$  and  $e$  refer to positive ions, negative ions and electrons, respectively. If the positive- and negative-ion diffusivities are comparable,  $D_p \approx D_n$ , the electric field vanishes, and diffusion is free for all charged species. Furthermore, the ambipolar electron diffusivity  $D_{ae}$  in an electronegative plasma is given by [45, 50]

$$D_{ae} \approx \left[ \frac{1 + 2(n_n/n_e)}{[(\mu_e/\mu_n) + 1] + 2(n_n/n_e)} \right] D_e. \quad (2)$$

In deriving equation (2) it was assumed that  $\mu_n = \mu_p$  and also that proportionality holds between the species density ratios and the corresponding gradients of density. Equation (2) indicates that  $D_{ae}$  becomes a larger fraction of the free electron diffusivity ( $D_e$ ) as the electronegativity ( $n_n/n_e$ ) increases. At the extreme of an ion–ion plasma,  $n_n \gg n_e$ , electrons diffuse with the maximum (free) diffusivity. A detailed account of the physics of the discharge evolution during a full pulse is given next.

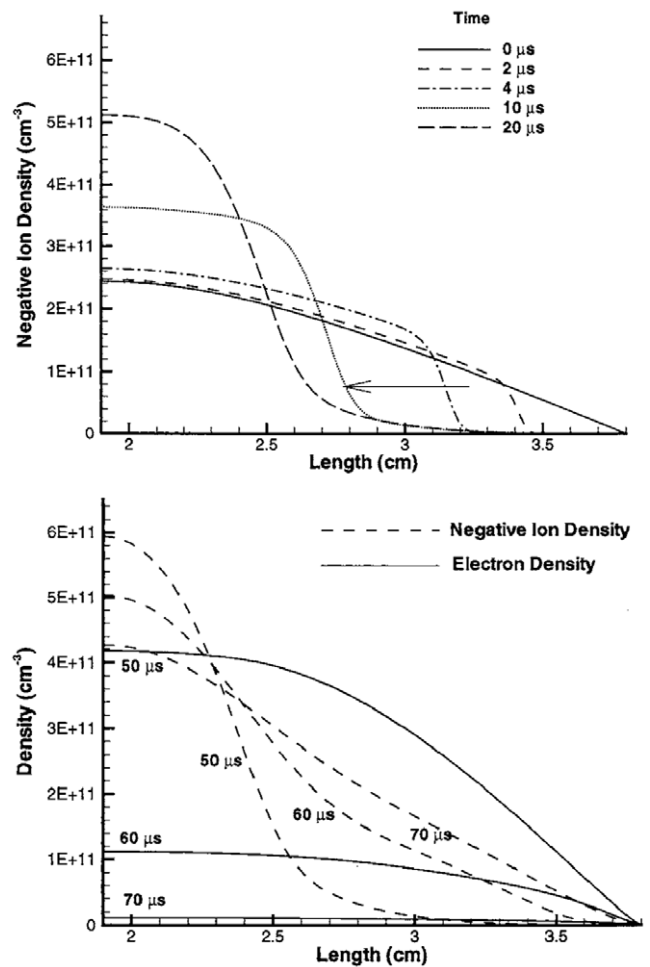


**Figure 6.** Predictions of a model of a high density pulsed chlorine plasma sustained between two parallel plates. (top) Space and time evolution of the negative-ion  $\text{Cl}^-$  density during the first  $20 \mu\text{s}$  of the *active glow*. (bottom) Space and time evolution of negative-ion and electron densities during the first  $20 \mu\text{s}$  of the *afterglow*. Conditions: power =  $1.0 \text{ W cm}^{-3}$ , pressure = 20 mTorr, pulse period =  $100 \mu\text{s}$ , and duty ratio = 50% ( $50 \mu\text{s}$  active glow,  $50 \mu\text{s}$  afterglow; source pulsing only). Only the right half of the 3.8 cm interelectrode space is shown (the centre of the plasma is at 1.9 cm and the right wall is at 3.8 cm). From [45] with permission.

### 3.1. Early active glow (0–15 $\mu\text{s}$ )

After the power is turned ON, the electron temperature rises sharply, overshooting its quasi-steady value, while the electron density increases more gradually. Initially ( $t = 0$ ), there are very few electrons remaining by the end of the afterglow of the previous pulse. In fact, the state of the plasma at  $t = 0$  (which is identical to that at  $t = T$ , provided that periodic steady-state has been reached) is an ion–ion ( $\text{Cl}_2^+$ ,  $\text{Cl}^-$ ) plasma in which the electrons diffuse almost freely (see equation (2)) due to the very weak electrostatic fields, determined by the ion temperature. As power is initially deposited to a small number of electrons, the electron temperature goes through a spike. As the electron temperature increases, the strength of the electrostatic field also increases, and negative ions, that had reached the wall late in the afterglow of the previous pulse, are squeezed towards the centre of the plasma (figure 6, top). As  $T_e$  increases, ionization comes into play which causes the electron density

to increase. The positive-ion density also increases during this time (figure 5). The negative-ion density goes through a local minimum at the beginning of the active glow due to detachment of negative ions by energetic electrons. The negative-ion density increases in the active glow (at the discharge centre) despite the fact that the production of negative ions by electron attachment at that location is less than the destruction of negative ions by electron detachment. This can be explained by the spatial movement of negative ions forming a front as they are squeezed towards the centre of the plasma. This drift flux of negative ions (remember that the electrostatic field is pointing towards the walls) more than compensates for the net loss of negative ions by the attachment–detachment processes. The negative-ion front is ‘self-sharpening’ because the electric field is stronger at the edge of the plasma as compared to that at the centre. The formation and movement of spatial fronts in the transient evolution of negative ions has been analysed theoretically by Kaganovich and Tsendin [55] and Kaganovich *et al* [39, 56, 57]. Squeezing of the negative ions towards the plasma centre leads to their entrapment in the plasma core and makes the negative-ion flux to the wall vanish (see sharp drop of negative-ion flux very early in the active glow in figure 7).

A spike in electron temperature immediately after the start of the active glow was observed experimentally by Malyshev *et al* [47, 51], as well as Ashida and Lieberman [52]. In contrast, no spike was reported by Meyyappan [53, 54]. Indeed, the presence and intensity of a spike depends on the electron density remaining at the end of the afterglow, which is the same as the electron density during the start of the active glow. The lower the starting electron density, the more pronounced the spike. In cases where the electron density does not decay significantly in the afterglow, there is no spike in  $T_e$  [53, 54].

### 3.2. Late active glow (15–50 $\mu\text{s}$ )

By the end of the early active glow, the electron density and electron temperature have reached a quasi-steady state, which is maintained until the end of the active glow. The positive-ion density is also approaching a quasi-steady value by the end of the active glow (figure 5). The quasi-steady values of  $n_e$ ,  $n_p$  and  $T_e$  correspond to the power level during the active glow, i.e. the peak applied power. However, the plasma is *not* at steady-state at that power level because the neutral gas (Cl atoms and Cl<sub>2</sub> molecules) composition responds to a much longer time scale, i.e. ms [1, p 380], compared to the pulse period. Indeed, for the typical case of pulsed plasma conditions examined, the neutral gas concentration responds to the time-average power, while  $n_e$ ,  $n_p$  and  $T_e$  respond to the instantaneous power (barring complications in chemically complex plasmas, see [58]).

### 3.3. Early afterglow (50–75 $\mu\text{s}$ )

Upon power turn OFF, electron heating stops, but electrons continue to lose energy by ambipolar diffusion to the walls and in collisions with neutrals (mainly inelastic at first), causing the electron temperature to plummet. After the electron energy falls below the smallest inelastic collision threshold, electrons can only lose energy in elastic collisions

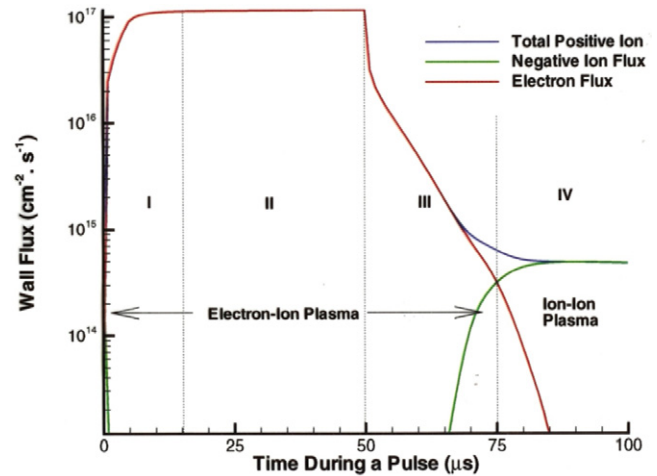


**Figure 7.** Time evolution of species wall fluxes predicted by a model of a high density pulsed chlorine plasma sustained between two parallel plates (plate separation = 3.8 cm). Power = 1.0 W cm<sup>-3</sup>, pressure = 20 mtorr, pulse period = 100  $\mu\text{s}$ , and duty ratio = 50%. Each pulse cycle is separated in four time windows: early active glow (I), late active glow (II), early afterglow (III) and late afterglow (IV). From [45] with permission.

with neutrals and by diffusion to the walls. Thus the rate of decay of  $T_e$  slows down. The precipitous fall of  $T_e$  is accompanied by disintegration of the electrostatic fields, allowing negative ions to back-diffuse towards the walls (figure 6, bottom). Ionization is quenched shortly after power OFF, while electron losses by attachment and diffusion to the walls continue. Therefore, the electron density decreases, albeit with a larger time constant compared to electron temperature decay. However, as the electrostatic field (which confines all but the high energy electrons in the plasma) disintegrates, the electron diffusion loss rate accelerates and the plasma becomes progressively more electronegative (i.e. the ratio  $n_n/n_e$  keeps increasing). A point is then reached at which the dominant negative charge carriers are the negative ions. At that point an ion–ion plasma forms which decays by ion–ion recombination and diffusion to the walls.

The negative ion and electron densities as a function of position at different times during the afterglow are shown in figure 6, bottom. The plasma is stratified by the end of the active glow,  $t = 50 \mu\text{s}$ , forming an electronegative core where almost all negative ions are trapped, and an electropositive edge without negative ions. The electron density profile is quite uniform in the electronegative core. This is because the electron ambipolar diffusivity is enhanced in the presence of negative ions (equation (2)) leading to milder concentration gradients. Plasma stratification has been studied extensively in CW electronegative discharges [1, 59].

In contrast to most electron-impact reactions, the rate coefficient of dissociative electron attachment to Cl<sub>2</sub> increases in the afterglow, as  $T_e$  decreases [52]. Thus, loss of electrons due to attachment accelerates in the afterglow. Eventually, however, the attachment rate decreases because of depletion of electrons. Global (volume-averaged) models of pulsed electronegative plasmas usually predict an increasing negative-ion density with time in the afterglow due to enhanced

attachment [60]. Spatially resolved simulations (figure 5) predict that the negative-ion density at the plasma centre decreases in the afterglow (except for a small increase in the early afterglow). This is because of a significant flux of negative ions out of the plasma centre (figure 6, bottom), as negative ions diffuse back towards the walls. In fact, depending on the spatial position at which the negative-ion density  $n_n$  is measured,  $n_n$  can increase or decrease as a function of time.

Figure 7 shows the charged species fluxes on the grounded electrode during a pulse period. The negative-ion flux becomes negligible (compared to the electron flux) very early in the active glow due to re-emergence of the electrostatic field, as the plasma is turned ON. The negative-ion flux remains suppressed (negative ions are trapped) until the late afterglow when an ion–ion plasma forms and negative ions are free to diffuse to the wall. While the negative-ion flux is zero, the electron and ion fluxes on the wall are equal to preserve electroneutrality. When an ion–ion plasma is present, the electron flux is negligible, making the positive and negative-ion fluxes equal. The positive-ion and electron fluxes decay rapidly a few  $\mu\text{s}$  into the afterglow due to the rapid decrease of electron diffusivity as  $T_e$  plummets. Furthermore, in the late afterglow, the rate of loss of electrons accelerates as the electron diffusivity  $D_{ae}$  approaches the free diffusion coefficient,  $D_e$  (equation (2)).

### 3.4. Late afterglow (75–100 $\mu\text{s}$ )

Electrons are lost in the early afterglow by ambipolar diffusion to the walls and dissociative attachment, while negative ions are still trapped in the reactor. Once the electron density  $n_e$  becomes less than  $1/2(m_i/m_e)n_n$ , negative ions become the dominant negative charge carrier in the plasma [45]. The electric field is now determined by negative ions instead of electrons and there is an abrupt transition from an electron-dominated plasma to an ion–ion plasma. The ion–ion plasma is characterized by weak electrostatic fields and a diffusive flux of negative ions to the walls. In figure 7, the transition from an electron–ion plasma to an ion–ion plasma is characterized by the electron flux becoming equal to the negative-ion flux at the walls ( $t = 75 \mu\text{s}$ ). The positive-ion flux, which initially overlaps with the electron flux in the early afterglow becomes equal to the negative-ion flux in the late afterglow. Experimental results reported by Smith *et al* [61] in the afterglow of an oxygen plasma show similar behaviour: the negative-ion flux was negligible in the early afterglow and abruptly increased by several orders of magnitude to become equal to the positive-ion flux in the late afterglow. The same behaviour was reported by Gutsev *et al* [62] and Kudryavtsev and Tsandin [63].

After the transition to an ion–ion plasma, electrons are no longer confined in the plasma and are lost at a faster rate which eventually approaches the limit of free diffusion of electrons to the walls (equation (2)) in the absence of electrostatic fields. The positive-ion and negative-ion densities decay together much more slowly due to ion–ion recombination and diffusion losses to the walls. The peak magnitude of the negative-ion flux is about two orders of magnitude less than the electron flux in the active glow. In the collisional plasma

under investigation this corresponds roughly to the ratio of the ambipolar diffusion coefficient to the ion diffusion coefficient, or, the ratio of electron temperature in the active glow ( $\sim 3 \text{ eV}$ ) to ion temperature ( $\sim 0.03 \text{ eV}$ ).

Ashida and Lieberman [52] also showed that extraction of negative ions becomes possible only when the sheath voltage or electrostatic fields collapse in the afterglow due to thermalization and loss of electrons. Once the electrons are lost, the negative-ion flux to the walls increases and becomes equal to the total positive-ion flux. They also showed that the coefficient for recombination of Cl radicals on the reactor walls played an important role in determining the extent of dissociation of  $\text{Cl}_2$  molecules in the plasma. The neutral composition, in turn, affected the rate of decay of electrons and the evolution of negative ions in the afterglow.

It should be mentioned that instead of a temporal afterglow as a result of source pulsing, one can have an equivalent *spatial afterglow* in a flowing plasma, sustained by a CW power source. In a spatial afterglow, time is replaced by downstream distance  $d$  from the plasma,  $t = d/u$ , where  $u$  is an average flow velocity. Far enough downstream of the plasma generation zone, the electron density can decay substantially to form an ion–ion plasma. For the plasmas of interest, electron decay is mainly by electron attachment to electronegative gases and diffusion to the walls of the reactor.

## 4. Pulsed plasma panoply

This section starts with the use of pulsed plasmas to study chemical reaction kinetics *in situ* (in the plasma itself). Then, the effect of pulsing on several plasma characteristics (charged and neutral species densities and fluxes, ion energy distributions (IEDs) on the plasma electrodes, and the EEDF) is discussed. The use of pulsed plasmas to extract negative ions is also discussed.

### 4.1. Measurement of reaction kinetics

Pulsed plasmas (usually source pulsing without bias) are often used to measure the kinetics of homogeneous or heterogeneous reactions under ‘realistic’ conditions, i.e. in the plasma itself [64–66]. Belostotsky *et al* [64] investigated the dynamics of negative-ion density in the positive column of a dc glow discharge in pure oxygen. They used laser photodetachment over a wide range of pressure (0.1–5 Torr) and current density (2–40  $\text{mA cm}^{-2}$ ). Using square wave modulation of the discharge current (i.e. power), the time evolution of the concentration of critical species in the discharge was analysed, to extract the rate coefficients of  $\text{O}^-$  detachment by atomic oxygen,  $\text{O}(^3\text{P})$ , and singlet molecular oxygen,  $\text{O}_2(a^1\Delta_g)$ , under plasma conditions. Hansen *et al* [65] studied the kinetics of formation and decay of excited fluorine atoms ( $\text{F}^*$ ), and CF and  $\text{CF}_2$  radicals in source modulated  $\text{CF}_4$  plasmas.  $\text{F}^*$  was monitored by optical emission spectroscopy and  $\text{CF}_x$  ( $x = 1, 2$ ) radicals were detected using laser induced fluorescence (LIF). Takahashi *et al* [66] used infrared diode laser absorption spectroscopy (IRLAS) to measure  $\text{CF}_x$  ( $x = 1, 2, 3$ ) radical densities in source power modulated (no

bias) ECR CHF<sub>3</sub> plasmas. The radical density varied with the duty ratio of the 100 ms PRF discharge. The polymer deposition rate (no bias) was the same on Si and SiO<sub>2</sub> surfaces and followed the same trend with the CF and CF<sub>2</sub> densities, decreasing with increasing duty ratio.

Booth *et al* [67] measured, using LIF, the spatial and temporal variation of CF and CF<sub>2</sub> radical concentrations in CF<sub>4</sub> capacitively coupled RF (13.56 MHz) plasmas at 50 and 200 mTorr, under fluorine rich conditions (no polymer deposition). The temporal variation was obtained by switching the plasma ON or OFF. This can be thought of as a limiting case of a pulsed plasma with very long active glow and afterglow, so that a steady state is obtained during both plasma ON and plasma OFF. They found that the Al powered electrode was a net source of these radicals whereas the Al grounded counter-electrode was a net sink. They concluded that CF<sub>x</sub> radicals were predominantly produced by CF<sub>x</sub><sup>+</sup> ions neutralizing, dissociating and reflecting off of the powered electrode. The different behaviour of the grounded electrode was explained based on the different energy and mass distribution of ions striking that electrode. In a companion study, Cunge and Booth [68] measured the CF<sub>2</sub> concentration profiles under fluorine starved conditions (polymerization). The F atom concentration was suppressed by loading the reactor with a Si wafer or by using C<sub>2</sub>F<sub>6</sub> instead of CF<sub>4</sub> plasma. They found that all surfaces in contact with the plasma were sources of CF<sub>2</sub> radicals. This led them to conclude that the CF<sub>2</sub> radical is not a direct precursor of polymer growth on the walls, as has been suggested in the literature [69]. Instead, CF<sub>2</sub> radicals form oligomers in the gas phase and these are the actual polymer deposition precursors.

Vempaire and Cunge [70] used a pulsed plasma to probe the kinetics of BCl radicals in the afterglow of a BCl<sub>3</sub>/Cl<sub>2</sub> ICP. In most of the afterglow, there is virtually no production of radicals by electron-impact reactions since the electron temperature quenches within several  $\mu$ s. Thus, the radical loss, occurring at much longer time scales by homogeneous chemical reactions as well as surface processes, can be studied. The authors estimated the rate coefficient of the reaction of BCl with Cl<sub>2</sub> to be  $5 \times 10^{-11} \text{ cm}^3 \text{ s}^{-1}$ , large enough to make this gas-phase reaction the main loss of BCl, despite the low pressure of 5 mTorr. The reaction probability of BCl on the reactor walls was estimated to be  $\gamma = 0.3 \pm 0.1$ . Cunge *et al* [71] studied radical-wall interactions during etching of silicon in Cl<sub>2</sub>/O<sub>2</sub> plasmas in industrial plasma reactors. They found that SiCl can stick on a SiOCl-coated reactor wall with a probability nearly 100%. SiCl<sub>2</sub> appeared to be much less reactive towards that wall. SiCl residing on the wall is oxidized in the presence of oxygen to form SiOCl. Using a pulsed plasma and following the evolution of radicals in the afterglow with time-resolved absorption measurements, they estimated the Cl recombination coefficient to be  $\sim 0.007$  on the SiOCl covered surface, and  $\sim 0.1$  on the clean wall (AlF<sub>3</sub>). They also found that, despite the low operating pressure of 20 mTorr, gas-phase reactions such as  $\text{SiCl} + \text{Cl}_2 \rightarrow \text{SiCl}_2 + \text{Cl}$  have a significant influence on the radical densities.

Kono *et al* [72] presented an experimental study of the variation of electron and negative-ion densities in pulsed

CF<sub>4</sub> plasmas at low power and pressure in the range 100–300 mTorr. In accordance with other investigators [45, 62], they observed enhanced loss of electrons in the afterglow due to the presence of negative ions. They also reported that loss of negative ions by detachment was comparable to that by negative-ion/positive-ion recombination in the active glow. The main species causing detachment was CF<sub>3</sub>, and dissociative electron attachment to CF<sub>4</sub> was the main channel to produce F<sup>−</sup> negative ions.

#### 4.2. Species densities

Source power modulation can influence not only the relative concentration of radicals but also the spatial distribution of these radicals (and of the precursor gas) in a plasma reactor. For example, as the feed gas flows through the plasma, the precursor is depleted by electron-impact dissociation. As a result, the etching or deposition rate may vary along the flow path of the gas. Power modulation can be used to alleviate such variations, thereby improving process uniformity. There are at least two ways power modulation can affect the spatial distribution of neutral species. (1) If the plasma power-OFF phase (afterglow) lasts for a time comparable to the gas residence time in the reactor, the reactor can be essentially refilled with fresh precursor gas during the afterglow. This minimizes spatial density variations of the precursor and improves uniformity. (2) If the duration of the active glow is short compared to the time it takes for the concentration gradients of the etch or deposition radicals (originating by e-impact dissociation of the precursor) to develop significantly, source pulsing again should improve uniformity [22, 27, 28].

The effect of source pulsing (pulse period 10s of ms) with no bias, on the radical concentration and etching rate of Si in a relatively high pressure (1 Torr) CF<sub>4</sub> plasma was simulated using a transport and reaction model [22]. The reactor was a parallel-plate single-wafer etcher with a showerhead electrode. Under conditions for which chemical etching was dominant, it was found that etch uniformity improved with power modulation, especially for low flow rates. In addition, by changing the duty ratio, the radical concentration ratios CF<sub>2</sub>/F and CF<sub>3</sub>/F were altered, which can impact selectivity. In an experimental investigation, Bodart *et al* [73] reported the effect of source pulsing (no bias) on the density of radicals in Cl<sub>2</sub> and HBr ICPs at 20 mTorr. For pulsing frequencies greater than 500 Hz, the radical (Cl and Br) density increased with duty ratio, and did not depend on the pulsing frequency. On the other hand, after the plasma was turned ON, the ion flux reached a steady state within 10s of  $\mu$ s. The authors concluded that, for not too high pulse frequencies (less than 10 kHz), the ion flux is roughly independent of duty ratio. Therefore, the ion-to-radical flux ratio could be controlled quasi-independently by varying the pulse frequency and duty ratio.

The time evolution of the electron density during source pulsing of an argon or chlorine ICP (no bias) was studied experimentally by Hebner and Fleddermann [46]. For a PRF of 10 kHz, the electron density reached a plateau (for duty ratios  $D > 50\%$ ) that corresponds to the CW plasma at the same power (figure 8(a)). The effect of power on electron

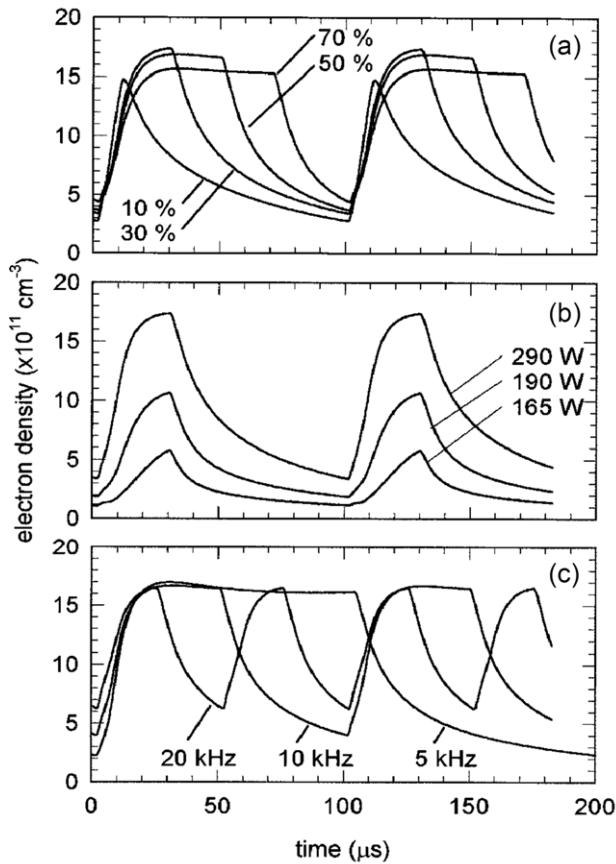


**Figure 8.** Time-dependent electron density in an argon ICP as a function of (a) duty ratio, (b) peak RF power and (c) PRF. In (a), the peak RF power was 300 W and the PRF was 10 kHz. In (b), the duty ratio was 30% and the PRF was 10 kHz. In (c), the peak power was 300 W and the duty ratio was 50%. In all cases, the pressure was 20 mTorr. From [46] with permission. Copyright 1997 AIP Publishing LLC.

density is shown in figure 8(b). Duty ratio  $D = 30\%$  is not enough to reach a plateau. However, the extrapolated plateau values scale linearly with power. Also, for a fixed duty ratio and peak power, the time-average power remains constant as the pulse period varies. Since the ‘power ON’ fraction of the cycle is longer than the time scale of electron density evolution, the same quasi-steady value of electron density is attained as the pulse period is varied (figure 8(c)). The situation is more complicated in chlorine discharges, however (figure 9). For example, in contrast to figure 8(a), the plateau electron density decreases with duty ratio (figure 9(a)). Increasing the PRF yields a decrease of the plateau value initially, and then an increase (figure 9(c)). These complications were attributed to changing plasma gas composition (ratio of Cl to  $\text{Cl}_2$  densities) as PRF and  $D$  were varied. Analytic expressions for the variation of electron temperature and density in the active glow and the afterglow under simplified conditions are given in [1, pp 369–81].

The  $\text{Cl}^-$  density profile evolution in a GEC reference cell, predicted by a plasma reactor simulation [74, 75], is shown in figures 10(a)–(f) [76]. At the start of a pulse, negative ions are present in the periphery (figures 10(a) and (b)) due to diffusion during the afterglow of the previous pulse. As

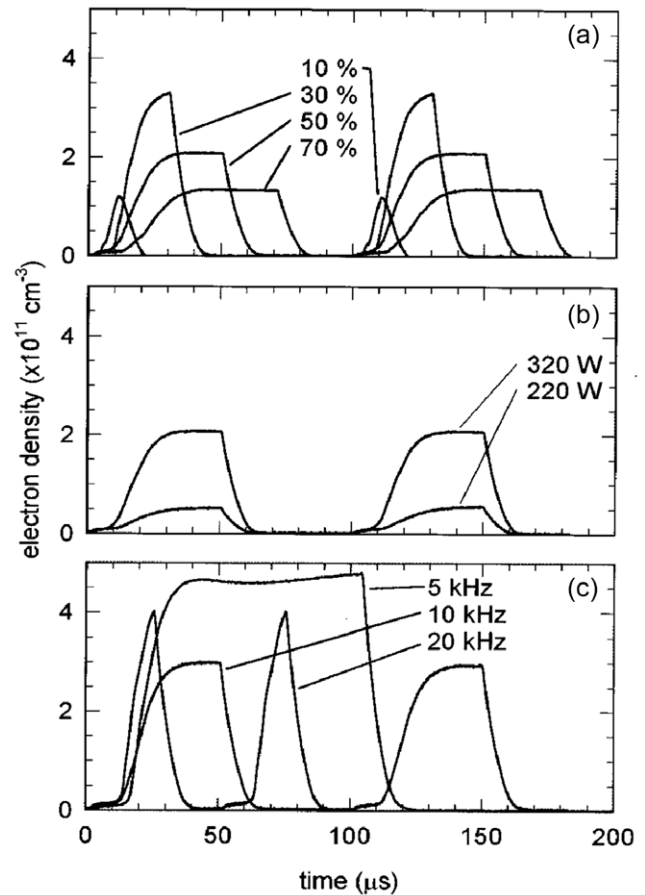


**Figure 9.** Time-dependent electron density in a chlorine ICP as a function of (a) duty ratio, (b) peak RF power and (c) PRF. In (a), the peak RF power was 320 W and the PRF was 10 kHz. In (b) the duty ratio was 50% and the PRF was 10 kHz. In (c), the peak power was 290 W and the duty ratio was 50%. In all cases, the pressure was 20 mTorr. From [46] with permission. Copyright 1997 AIP Publishing LLC.

the electron temperature and electron density start to increase, the ambipolar electric field also increases, causing negative ions to be squeezed into the plasma (figures 10(c) and (d)). The squeezing of negative ions is stronger near the quartz window since the electron temperature (therefore the field) is larger in that region. Because there is negligible flux of negative ions to the wall during the active glow, the quasi-steady state of negative-ion profile (see also figure 6) is sustained by a balance between production processes such as attachment and destruction processes such as detachment and ion–ion recombination. Later in the afterglow, negative ions start diffusing back towards the walls, as the electric field diminishes. Their diffusion is almost free (almost no electric field) after an ion–ion plasma forms.

Agarwal *et al* [77] simulated silicon etching in an Ar/ $\text{Cl}_2$  (20/80) ICP at 10 mTorr and 100 sccm total flow. Three situations were studied, under the following base case conditions: (I) pulsed source power (300 W peak) and CW bias power (100 W), (II) CW source power (300 W) and pulsed bias power (100 W peak), and (III) synchronous (in phase) pulsing of both source power and bias power (300 W peak source power, 100 W peak bias power). In all cases of pulsing

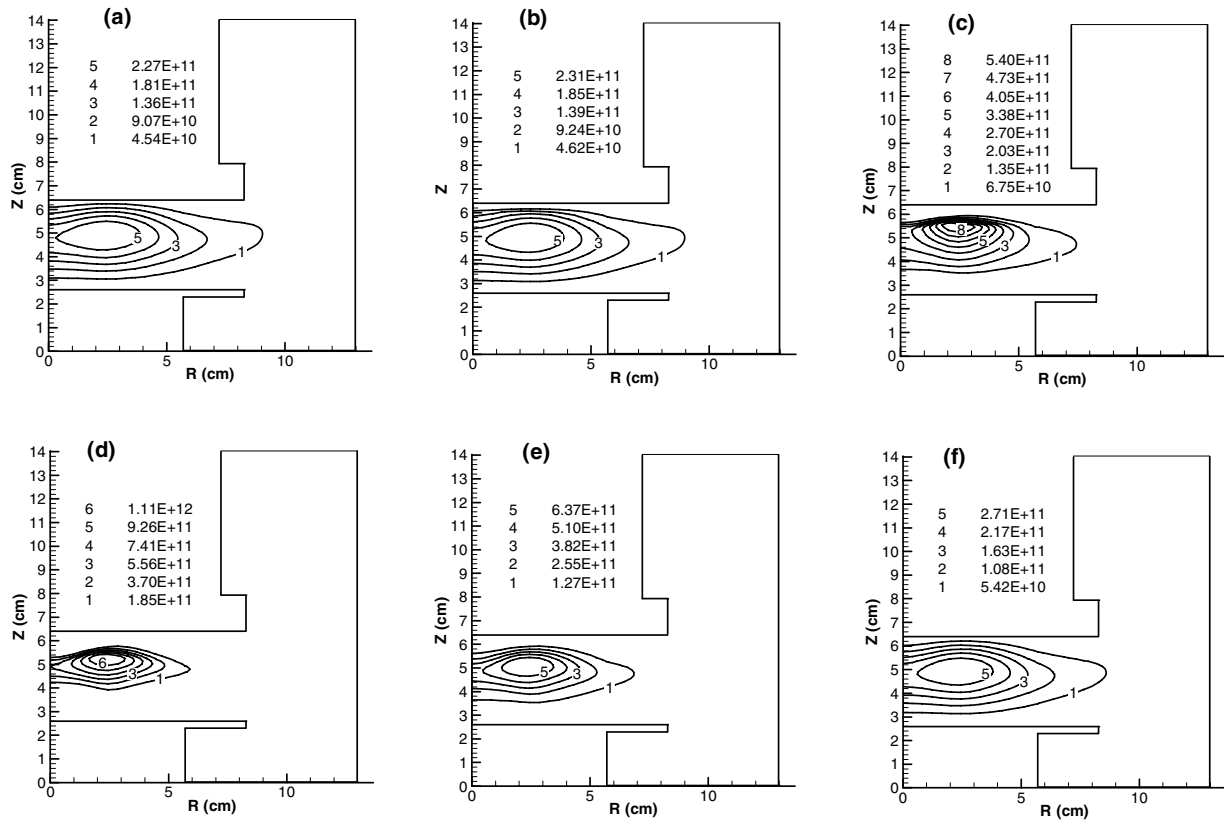


**Figure 10.** Negative-ion  $\text{Cl}^-$  density ( $\text{cm}^{-3}$ ) evolution in a GEC reference cell (inductive coupling) with source pulsing (no substrate bias). Pressure = 20 mTorr, peak power = 320 W, PRF 10 kHz, and duty ratio 50% ( $50 \mu\text{s}$  active glow,  $50 \mu\text{s}$  afterglow): (a)  $0 \mu\text{s}$ , (b)  $1 \mu\text{s}$ , (c)  $5 \mu\text{s}$ , (d)  $50 \mu\text{s}$ , (e)  $60 \mu\text{s}$  and (f)  $90 \mu\text{s}$  from the start of the active glow, which is at  $t = 0$ . The density values corresponding to each contour are given as insert in each panel. From [76] with permission. Copyright 2002 American Vacuum Society.

the pulse frequency was 5 kHz with 50% duty ratio. The time evolution of the spatially averaged (over the reactor volume) electron, negative ion ( $\text{Cl}^-$ ), and dominant positive-ion ( $\text{Cl}_2^+$ ) densities as well as the electron temperature are shown in figure 11 for cases I (source), II (bias) and III (sync). Generally, bulk plasma quantities (e.g. species densities) are controlled by the source power since, when the bias power is pulsed (and the source power is CW, i.e. case II), there is no modulation of the densities or the  $T_e$ . If bias power had an effect, these quantities would change over the pulse period. For the same reason, case I and case III result in very similar profiles. However, there is a slight heating of electrons by the RF bias during the afterglow in case I (pulsed source but CW bias), that results in warming of electrons late in the pulse (figure 11(d)). Regarding the negative ions, their density decreases in the active glow, in cases I and III, as energetic electrons detach negative ions. In contrast, cool electrons readily attach in the afterglow leading to increasing (albeit very slowly) negative-ion density. In case II (bias), the electrons are energetic throughout the pulse, and the negative-ion density has a lower constant value.

Brihoum *et al* [58] measured the flux and energy distribution of ions bombarding the substrate electrode in an ICP at 10 mTorr. The source power (750 W peak) was pulsed at 1 kHz and different duty ratios. In noble gas (Ar, He) plasmas, the ion flux increased upon power turn ON and, for long enough active glow duration, reached a quasi-steady state value identical to that in a CW plasma at the same power. This

matches the argon plasma results of Hebner and Fleddermann [46]. Thus, for pulse periods long compared to the ion density rise time of  $\sim 100 \mu\text{s}$ , the ion flux should be independent of the duty ratio. This was in contrast to  $\text{Cl}_2/\text{SiCl}_4$  plasmas for which the pulsed plasma ion flux was much lower than that of the CW plasma, and it was a strong function of the duty ratio. This was attributed to plasma chemical composition and electronegativity changing upon variation of the duty ratio. Furthermore, when the substrate was biased *synchronously* (in phase) with the source, the substrate was bombarded with a low flux of high energy ions, resembling a CCP reactor. The authors concluded that pulsing the plasma can offer a wide latitude in the operating parameter space that may have processing advantages.

Wagner and Katsch [78] measured the spatio-temporal profiles of negative oxygen ions ( $\text{O}^-$ ) in a pulsed ICP (source pulsing) in mixtures of oxygen with Ar, Kr or Ne. An increase in the negative-ion density was observed in the early afterglow suggesting that negative ions were formed by a process that becomes more important as the electron temperature decreases. The authors surmised that negative ions were produced by dissociative attachment of electrons to highly excited metastable oxygen molecules. This suggestion was made earlier by Hayashi and Kadota [79], and was implemented in a global model of pulsed oxygen discharges by Panda *et al* [80]. Wagner and Katsch also found that noble gas metastable atoms play negligible role in the formation of negative ions in the afterglow.

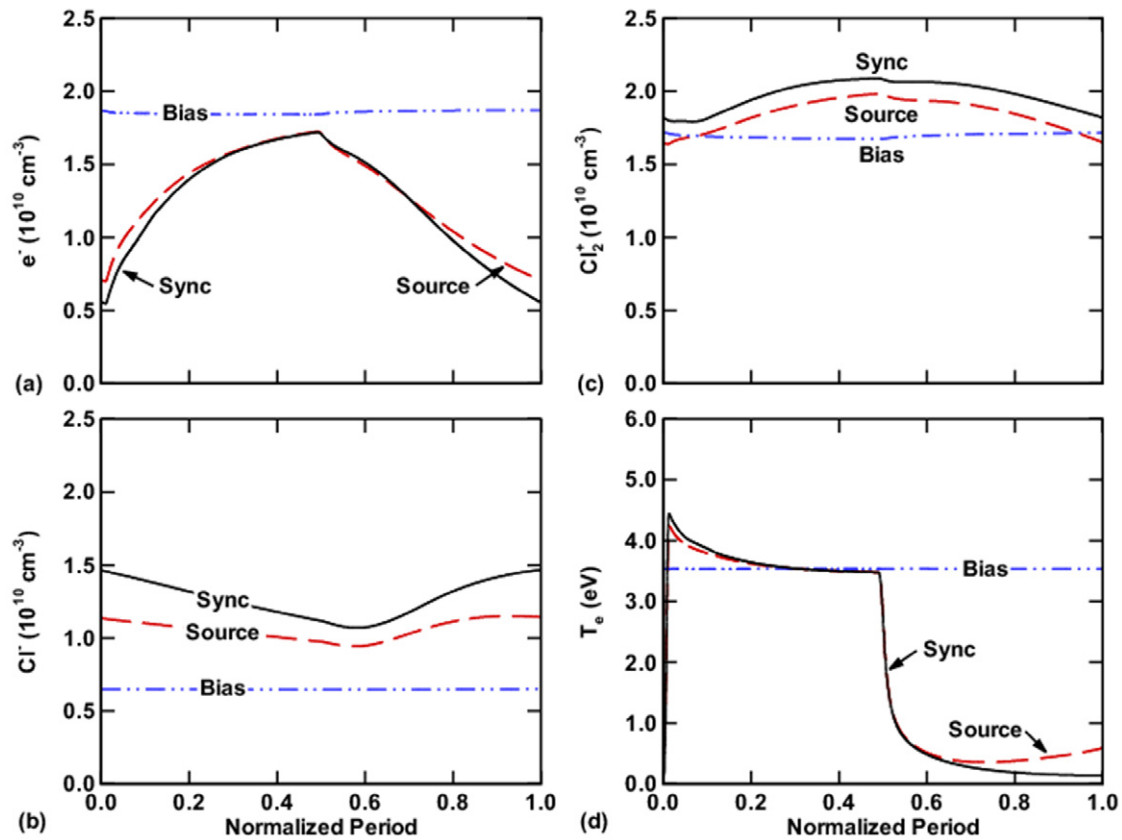


**Figure 11.** Spatially averaged plasma properties as a function of time during a pulse for different pulsing modes (source, bias, and synchronous without phase shift): (a) electron density, (b)  $\text{Cl}^-$  density, (c)  $\text{Cl}_2^+$  density and (d) electron temperature. Ar/ $\text{Cl}_2$  = 80/20 ICP at 10 mTorr, 100 sccm, 300 W peak source power, 100 W peak bias power, 5 kHz PRF, and 50% duty ratio. From [77] with permission. Copyright 2011 American Vacuum Society.

Useful insights on the time evolution of species densities and electron temperature may be obtained by global (volume-averaged or zero dimensional) models. These models are popular because of their simplicity and fast execution time. In global models, plasma parameters are assumed to be spatially uniform and the sheath thickness is assumed to be negligible, allowing the plasma-sheath edge to be at the geometrical location of the wall. This assumption is better in high density plasmas where the sheath is thin (small Debye length). Species mass balance equations, and an energy balance are solved simultaneously to determine the species density and electron temperature (often assuming Maxwellian EEDF). Ashida and Lieberman studied both electropositive (argon [81]) and electronegative ( $\text{Cl}_2$ ) discharges [52]. They found higher (more than 2 times) time-average plasma density in a 5 mTorr pulsed Ar discharge, compared to a CW discharge at the same time-average power. Properties of a chlorine discharge were found to depend on the wall recombination probability of Cl atoms, which determined the electronegativity of the discharge. The afterglow duration had to be above a critical value to allow extraction of negative ions. The negative-ion density  $\text{Cl}^-$  increased slightly during the active glow, exhibiting a shallow maximum in the afterglow, due to dissociative attachment of electrons with  $\text{Cl}_2$  to produce  $\text{Cl}^-$ . Global models of pulsed plasmas in chlorine were also reported by Meyyappan [54], Yokozawa *et al* [82],

and Thorsteinsson and Gudmundsson [60], among others. Meyyappan [53] also presented a global model in  $\text{SF}_6$  while Lee *et al* [83] and Panda *et al* [80] studied pulsed plasmas in oxygen. Pulsed hydrogen discharges have also received considerable attention [84, 85] in relation to production of negative ions,  $\text{H}^-$ . Unfortunately, global models cannot capture the formation and propagation of negative-ion fronts. These fronts can impact the time evolution of the negative-ion density, making it a sensitive function of the *spatial* location in the reactor. For example, depending on the spatial location at which the negative ions are monitored, the negative-ion density can increase or decrease in the afterglow. Also, Monahan and Turner [86], found the assumption of Maxwellian EEDF to be a significant limitation of global models.

#### 4.3. Extraction of negative ions

Negative ions are trapped in CW plasmas, but can be extracted from the late afterglow of pulsed plasmas, and accelerated by applying a positive dc bias on the substrate electrode or a negative dc bias on a BE. Samukawa *et al* [87] used pulsed  $\text{Cl}_2$  or  $\text{SF}_6$  ICPs to extract negative ions by applying a positive dc bias on the substrate electrode, late in the afterglow, when an ion-ion plasma had formed. The extraction electrode had high aspect ratio (10:1) through holes. Negative ions with directed velocity perpendicular to the substrate entered the

holes and suffered grazing angle collisions with the internal wall of the holes, turning into fast neutrals. This concept of ion neutralization to produce energetic neutral beams was also explored by Panda *et al* [88]. Another example of extraction and neutralization of negative ions involves  $\text{H}^-$ . Hydrogen negative ions are produced using pulsed plasmas in  $\text{H}_2$  [84, 85]. Highly excited vibrational states of molecular hydrogen are formed during the active glow, which undergo dissociative attachment with cool electrons in the afterglow, producing negative ions. These ions are accelerated to 10s–100s of keV and are neutralized before being injected in fusion reactors to assist in plasma heating.

Kanakasabapathy *et al* [89] used molecular beam mass spectrometry to study alternating extraction of positive and negative ions out of a 1 mTorr, 300 W (peak power) pulsed  $\text{Cl}_2$  plasma (PRF = 1 kHz, 50% duty ratio). A sinusoidal bias voltage (225 V peak, 100 kHz) was applied to the substrate electrode during the afterglow of the pulsed plasma (synchronous biasing). Ions were detected by a differentially pumped mass spectrometer located behind the substrate. Results are shown in figure 12. The left half of figure 12 corresponds to the active glow (0–500  $\mu\text{s}$ ) and the right half to the afterglow (500–1000  $\mu\text{s}$ ). Figure 12(a) shows  $\text{Cl}^-$  peaks (designated by letters A, B, C, ..., I) alternating with  $\text{Cl}_2^+$  peaks (designated by numbers 1, 2, 3, ..., 9). Figure 12(c) shows that the  $\text{Cl}^-$  peaks correspond to the positive swing of the bias voltage while the  $\text{Cl}_2^+$  peaks correspond to the negative swing of the bias voltage. This implies the existence of an ion–ion plasma. Apparently the bias applied in the afterglow was not high enough to heat the remaining electrons and re-establish a potential well deep enough to trap the negative ions [51, 90]. The intensity of the peaks decays as a function of time, as the ion–ion plasma decays by ion–ion recombination and diffusion to the walls. Formation of an ion–ion plasma is corroborated by figure 12(e) showing that the electron density (measured by both Langmuir probe (LP) and microwave interferometry) vanishes  $\sim 15 \mu\text{s}$  after power is turned OFF (giving way to an ion–ion plasma). Figure 12(a) also shows the  $\text{Cl}_2^+$  signal going through a peak in the early active glow, only to decay shortly thereafter as molecular chlorine is dissociated in the plasma. The  $\text{Cl}_2^+$  signal is delayed by  $t_{\text{TOF}} = 50 \mu\text{s}$  corresponding to the time of flight through the mass spectrometer. The  $\text{Cl}^+$  peak, in contrast is building up during the active glow (figure 12(b)). The  $\text{Cl}^+$  signal decays in the afterglow due to charge exchange with  $\text{Cl}_2$  to form  $\text{Cl}_2^+$ . The nuances of negative-ion extraction from a pulsed plasma were reported by Overzet *et al* [91]. The authors discussed conditions under which negative ions can be extracted from a plasma, and the dependence of negative-ion flux on pulse modulation frequency.

Ahn and co-workers [48] studied source power modulated Ar and  $\text{Cl}_2$  ICPs. For otherwise identical conditions, the electron density decayed much faster in chlorine compared to Ar, because chlorine has an additional sink of electrons via dissociative attachment to  $\text{Cl}_2$ . The authors observed suppression of notching in poly-Si gate structures when a +35 V bias was applied during part of the afterglow. The  $\text{Cl}^-$  density, measured by photodetachment, increased monotonically in the afterglow. However, as mentioned above,

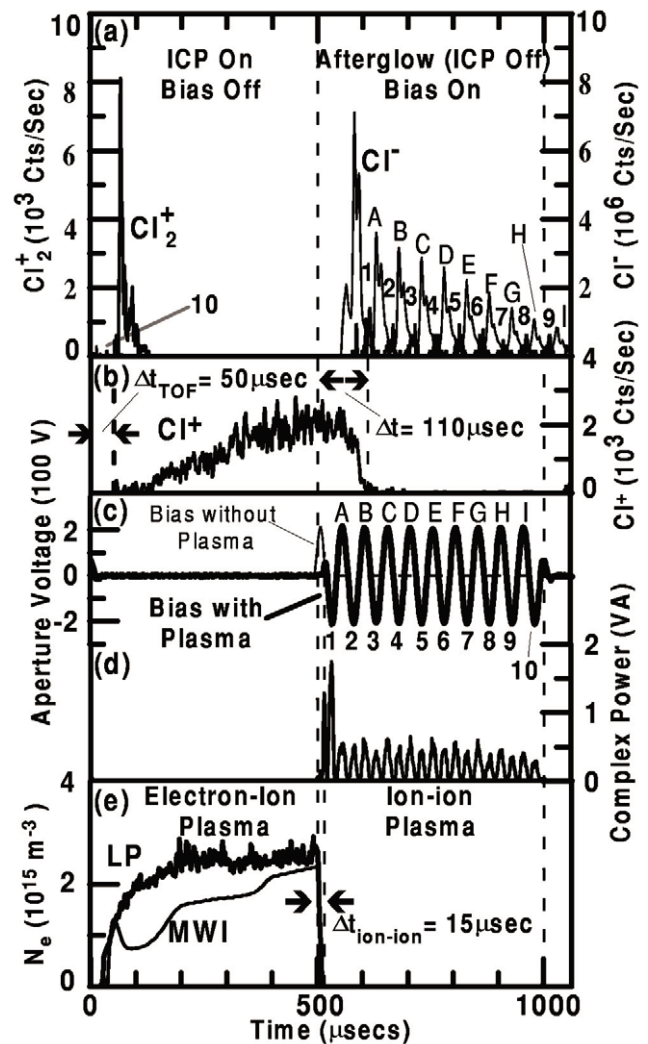


**Figure 12.** Alternating extraction of positive and negative ions from a pulsed chlorine ICP (1 mTorr, 300 W peak source power, 1 kHz PRF, 50% duty ratio, i.e. plasma source was ON during 0–500  $\mu\text{s}$ , and OFF during 500–1000  $\mu\text{s}$ ). A 100 kHz bias was applied to a substrate electrode synchronously during the entire afterglow of the ICP (500–1000  $\mu\text{s}$ ). (a) Time evolution of molecular chlorine positive ions ( $\text{Cl}_2^+$ ) and atomic chlorine negative ions ( $\text{Cl}^-$ ) bombarding the substrate electrode, (b) time evolution of the  $\text{Cl}^+$  signal, (c) voltage on the substrate electrode, (d) complex power and (e) electron density evolution (measured with a LP and with microwave interferometry (MWI)), during a pulse. From [89] with permission. Copyright 2001 AIP Publishing LLC.

the time behaviour of negative-ion density depends on the spatial position where the measurement is taking place.

Maeshige *et al* [92] used a ‘test structure’ to study injection of negatively charged species (electrons and negative ions) in a power-modulated dual-frequency capacitively coupled reactor in Ar– $\text{CF}_4$  (90%–10%) gas mixtures at 25 mTorr. The source power (at 100 MHz) was square-wave modulated 10  $\mu\text{s}$  ON and 10  $\mu\text{s}$  OFF. The substrate bias voltage was negative during source power ON, but it swung temporarily positive during the afterglow (source power OFF). A test structure, resting on the substrate electrode, was fabricated by opening holes in a  $\text{SiO}_2$  layer grown on a silicon wafer. The voltage of the silicon wafer surface at the bottom of the hole (charging voltage) was

monitored. Under CW operation a large positive charging voltage was measured due to differential charging of the holes. Under pulsed plasma conditions, the charging voltage was significantly reduced. The authors hypothesized that during the positive swing of the substrate voltage, there was an electric field reversal ( $E$ -field pointing towards the plasma) which caused injection of negative species (electrons and negative ions) that neutralized the positive charge accumulated at the hole bottom. Time-resolved optical emission spectroscopy showed a strong signal at the sheath edge during the positive swing of the substrate voltage corroborating the evidence of energetic electrons during that time. There was no charge neutralization observed when the substrate voltage swung positive during the active glow of the Ar-CF<sub>4</sub> plasma or in the afterglow of a 100% argon plasma. Apparently there was no field reversal occurring in these cases [92, 93].

The decay of electronegative plasmas in the afterglow of pulsed discharges under a variety of situations has been studied by Kaganovich *et al* [56]. The time needed for negative ions to reach the wall is of importance for applications based on negative-ion extraction. For a three-component plasma (electrons, negative ions and positive ions), when all three species have the same temperature  $T_i$ , the following limiting cases were distinguished:

- (a) For diffusion dominated afterglow (neglecting plasma chemical processes such as attachment, detachment, ion-ion recombination, etc), the time needed for negative ions to reach the wall is given by,

$$t_{n,out} = \frac{\Lambda^2}{2\mu_i T_i} \ln\left(\frac{p_0}{n_0}\right) \quad (3)$$

where  $\Lambda$  is the effective diffusion length,  $\mu_i$  is the ion mobility, and  $p_0$ ,  $n_0$  are the positive- and negative-ion densities, respectively, at the beginning of the afterglow. This equation has practical significance, despite the assumption of equal temperatures among the three charged species, since the electron temperature normally plummets within several  $\mu s$  in the afterglow to near the other species temperature. Equation (3) indicates that the time it takes for the negative ions to reach the wall is shorter for higher electronegativity (as electronegativity increases,  $n_0$  gets closer to  $p_0$  and  $t_{n,out}$  decreases. (note that this equation in [49] is missing the logarithm (ln), by oversight).

- (b) When attachment dominates in the afterglow, the corresponding time is [56]

$$t_{n,out} = \frac{1}{v_{att}} \ln\left(\frac{v_{att} \Lambda^2 n_{e0}}{2\mu_i T_i p_0}\right) \quad (4)$$

where  $v_{att}$  is the attachment frequency ( $v_{att} = k_{att} [Cl_2]$ ), and  $n_{e0}$  is the electron density at the beginning of the afterglow.

- (c) When detachment of negative ions is important in the afterglow (e.g. case of O<sub>2</sub> plasma where O(<sup>3</sup>P) atoms and O<sub>2</sub>(<sup>1</sup> $\Delta_g$ ) molecules can detach negative ions O<sup>-</sup>, see [64]), the situation depends critically on the product of the detachment frequency  $\gamma_{det}$  and the negative-ion diffusion time,  $\tau_d$  [90]. If  $\gamma_{det} \tau_d > 2$ , negative ions detach

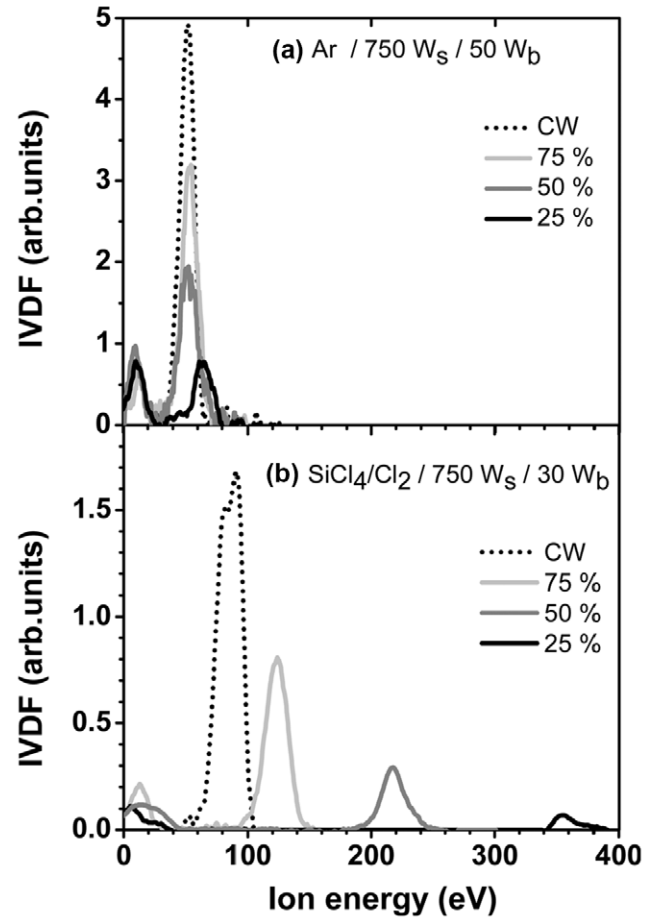


**Figure 13.** Time-average IVDFs for different duty ratios in (a) 50 sccm argon and (b) 60 sccm SiCl<sub>4</sub>/20 sccm Cl<sub>2</sub>, synchronously pulsed ICPs. In both cases the source power was 750 W, the pulsed repetition frequency was 1 kHz, and the pressure was 10 mTorr. The bias power was 50 W in (a) and 30 W in (b). The CW IVDFs under otherwise the same conditions are also shown. From [58] with permission. Copyright 2013 American Vacuum Society.

during their diffusion to the wall, and the resulting electrons generate an electric field, trapping the negative ions. If  $\gamma_{det} \tau_d < 2$ , detached electrons disappear by free diffusion, and the negative-ion flux to the wall equals the positive-ion flux.

- (d) When  $T_i \ll T_e$ , a negative-ion front propagates in the afterglow with a constant velocity (assuming constant  $T_i$  and  $T_e$ ),  $V_{if} = \sqrt{4D_i Z_{e,loss}}$ , where  $D_i$  is the ion diffusivity and  $Z_{e,loss}$  is the electron loss frequency [57].

#### 4.4. Ion energy and angular distributions

Brihoum *et al* [58] measured time-average ion velocity distribution functions (IVDFs) for different duty ratios in Ar and SiCl<sub>4</sub>/Cl<sub>2</sub> ICPs with synchronous pulsing of the source and bias powers (figure 13). The IVDF of the corresponding CW plasma was also measured. Figure 13(a) shows that the IVDF of the CW argon plasma has a single peak at ~50 V. This is according to expectations given a plasma potential of ~15 V and a dc self-bias of -40 V developed on the substrate electrode in the CW plasma. The presence of a single peak

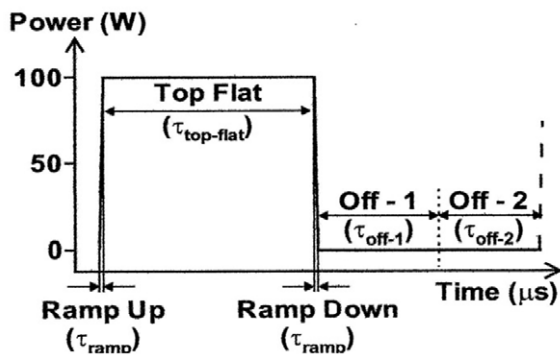


**Figure 14.** Schematic of a pulsed power waveform with finite ramp-up and ramp-down times. Five distinct phases during a pulse are identified: ramp-up, top-flat, ramp-down, off-1 and off-2. From [77] with permission. Copyright 2011 American Vacuum Society.

for the CW plasma implies that the ion transit time is larger than the period of the applied field. The IVDF of the pulsed plasma exhibits two peaks. The higher energy peak is due to the fraction of the cycle when the synchronous bias is applied. The area under this peak scales with duty ratio. The location of this peak shifts to slightly lower energy as the duty ratio increases, because of the slightly higher ion current as duty ratio increases. The lower energy peak ( $\sim 15$  eV) is due to the afterglow fraction of the cycle. The IVDFs of the reactive gas plasma (figure 13(b)) are very different. The CW IVDF peaks at 90 eV. This is because the ion flux is much lower in this plasma so that a larger dc bias (in absolute value) develops to dissipate the applied bias power. The IVDF of the pulsed plasma shows that the peak energy shifts to higher values as duty ratio decreases because of the lower ion current with decreasing duty ratio.

Agarwal *et al* [77] simulated silicon etching in an Ar/Cl<sub>2</sub> (20/80) ICP at 10 mTorr and 100 sccm total flow, using synchronous (in phase) pulsing of both source power (300 W peak) and bias power (100 W peak). The pulse frequency was 5 kHz with 50% duty ratio. The duration of both ramp-up and ramp-down of the power (figure 14) was  $2 \mu\text{s}$ . The afterglow was divided in an early afterglow stage (Off-1) and a late afterglow stage (Off-2). The calculated IED is shown in figure 15. Figure 15(a) shows the full IED while figures 15(b)–(d) show the ‘component’ IEDs during distinct phases of a pulse cycle: ramp-up and ramp-down (b), top-flat (c), and power-off phases (d). The full IED is a weighted superposition of the component IEDs. The peak with energy  $\sim 5$  eV in figure 15(a) corresponds to the afterglow when both source and bias power are OFF. The seemingly bimodal peak around 100 eV is due to the top flat phase of the pulse (see figure 15(c)). There is also a weak peak at  $\sim 250$  eV corresponding to the early stages of power turn ON. Because the ion density has diminished over the afterglow of the previous pulse, the bias voltage on the electrode briefly exceeds the quasi-steady-state value (i.e.  $\sim 100$  V) to maintain the power deposition at 100 W. The component IED corresponding to the ramp-up and ramp-down of the power is shown in figure 15(b). This component contributes to the widening of the base of the main peak (at  $\sim 100$  eV) of the full IED (compare

figures 15(a) and (c)). Furthermore, the authors employed a Monte Carlo simulation to follow the profile evolution of high aspect ratio features etched in Si. Using pulsed source power (300 W peak) and CW bias power (100 W), resulted in the highest etching rate, but also in potentially more damage due to energetic ion bombardment, especially at the start of the active glow. Power compensation (i.e. using the same *time-average* power when pulsing, versus the CW case, as opposed to using the same peak power) enhanced the etching rate while had minor effect on the IED. It was concluded that CW source power (300 W) and pulsed bias power (100 W peak) or synchronous (in phase) pulsing of both source power (300 W peak) and bias power (100 W peak) with power compensation, may be used to maintain throughput while minimizing damage.

Agarwal *et al* [94] simulated the effect of simultaneous source and bias pulsing in plasma etching of Si using an Ar/Cl<sub>2</sub> (80/20) ICP at 10 mTorr. Other conditions were 100 sccm total flow, 300 W peak source power (13.56 MHz), 100 W peak bias power (also at 13.56 MHz), 5 kHz pulsing frequency (200  $\mu\text{s}$  period), the same duty ratio for both source and bias, and zero phase shift between the two. Rise and fall times for the power pulse were  $2 \mu\text{s}$  each. Figure 16 shows the IEAD of the dominant ion, Cl<sub>2</sub><sup>+</sup>, for each distinct phase of the pulse (see figure 14), for three duty ratios (25%, 50% and 75%). The corresponding RF bias voltage required to achieve the target peak power of 100 W, and the resulting dc self-bias voltage on the electrode, are shown in figure 17. At time zero, the power turns ON, heating the electrons left over from the previous pulse. Because of the low electron density at the beginning of the pulse, the sheath is relatively thick and most ions do not acquire the full sheath potential. The dc bias overshoots before reaching a quasi-steady state during plasma ON. As the plasma density increases in the top-flat phase, and the sheath becomes thinner, the time it takes ions to cross the sheath becomes commensurate to the RF period, yielding a bimodal IED. Since the ion energy is on average higher during this phase of the pulse, the ion angular distribution (IAD) becomes tighter. The ion energy is a bit higher during power ramp-down compared to ramp-up because the dc blocking capacitor takes some time before discharging, keeping the average dc bias more negative. During the power OFF phase of the cycle, the electric fields disintegrate and ions bombarding the electrode have low energy and wide angular distribution. Increasing the duty ratio leads to lower ion energies. This is because the electron density at the beginning of a pulse is higher as the duty ratio increases. Thus the dc bias required to deposit the same peak power of 100 W is lower.

Subramonium and Kushner [95] simulated extraction of negative ions from a pulsed ICP under the following base case conditions: Ar/Cl<sub>2</sub> (variable composition) plasma at 10 mTorr, 100 sccm, 450 W peak source power (10 MHz), 10 kHz pulsing frequency (100  $\mu\text{s}$  period), and 50% duty ratio. When, in addition, 250 W CW bias power (also at 10 MHz) was applied to the substrate electrode, no negative ions could be extracted. This was because the bias power heated the electrons, especially in the late afterglow, yielding a sheath voltage that could not be overcome by negative ions [51]. However, negative ions could be extracted when pulsed (100 V

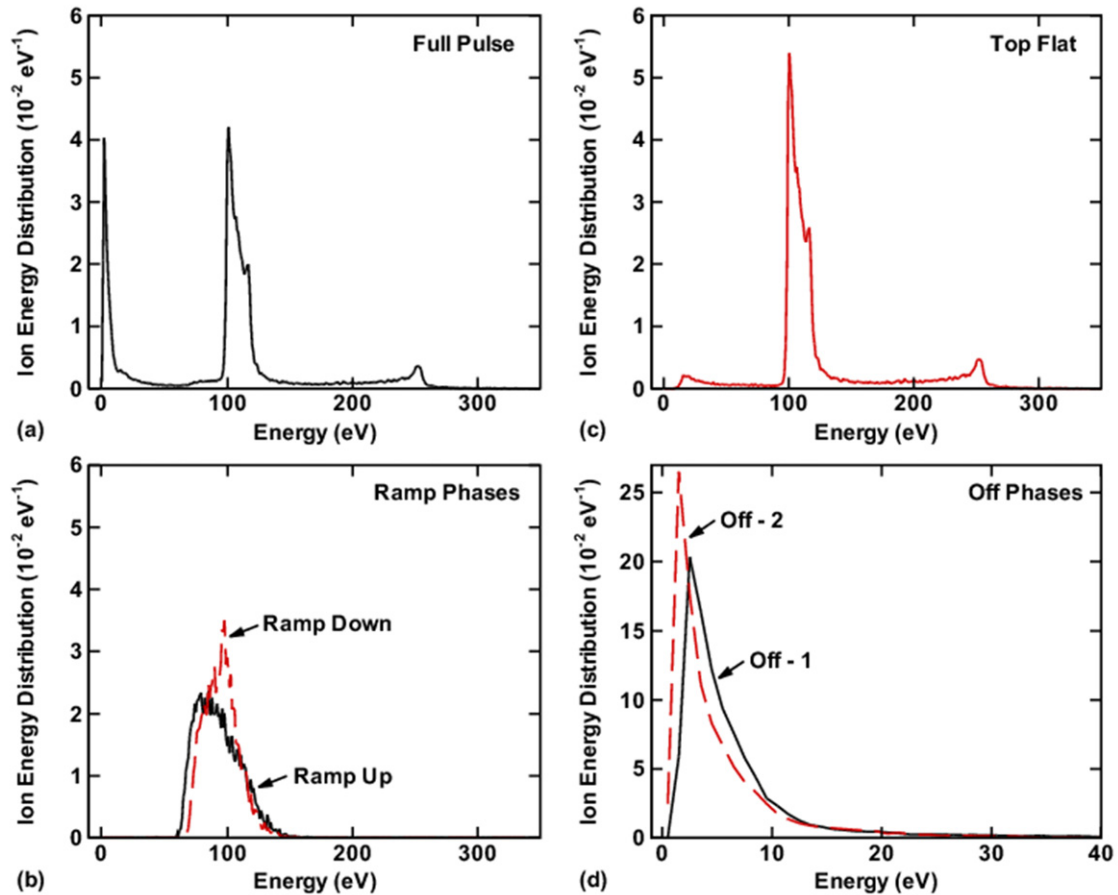


**Figure 15.** IEDs, integrated over the angle, during distinct phases of a pulse (figure 14) for synchronous biasing without phase difference: (a) full pulse average. IED is multi-peaked with each peak corresponding to distinct phases of the pulse; (b) ramp-up and ramp-down (each  $2 \mu\text{s}$  long); (c) top-flat; and (d) off-1 and off-2. Conditions: Ar/Cl<sub>2</sub> = 80/20, 10 mTorr, 100 sccm, 300 W peak ICP power, 100 W peak bias power and 5 kHz pulse frequency, 50% duty ratio. From [77] with permission. Copyright 2011 American Vacuum Society.

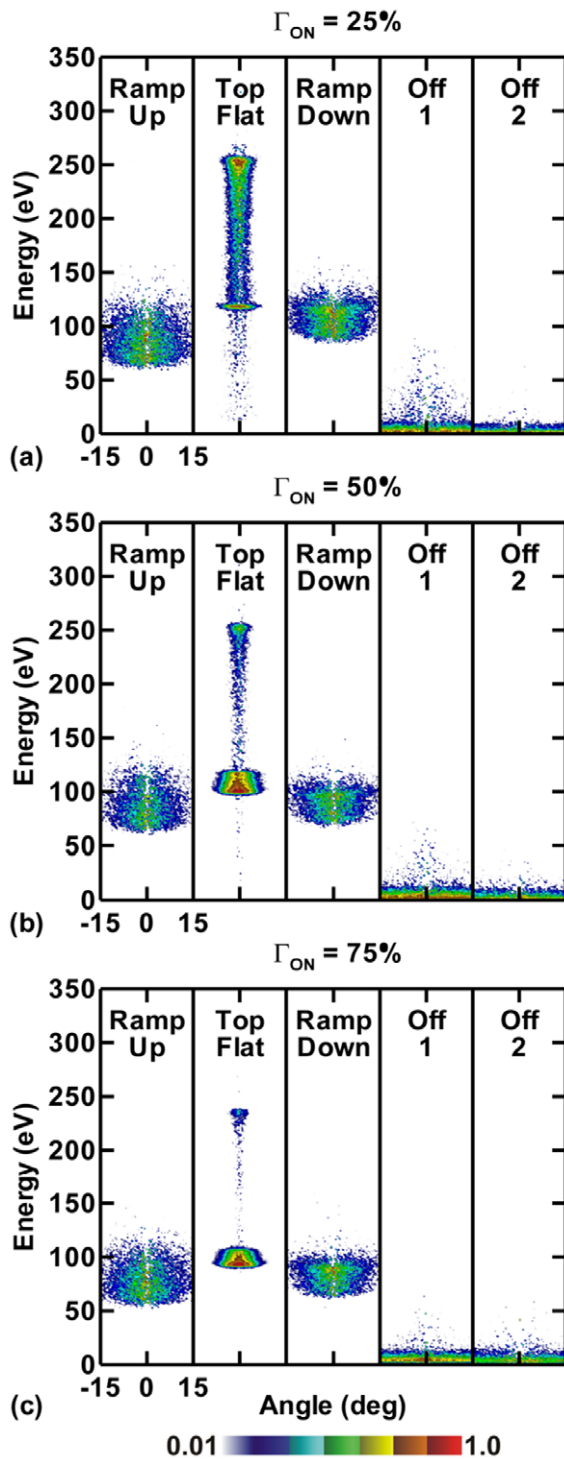
RF voltage, 6.67 kHz pulsing frequency, 33% duty ratio) bias power was applied during the last  $50 \mu\text{s}$  of the afterglow and the first  $10 \mu\text{s}$  of the active glow. The authors found that the amplitude of the applied voltage and the duration of the bias are key to obtaining negative-ion extraction from pulsed ICPs. For 50 or 100 V bias voltages at 10 MHz, ions arrived on the substrate with thermal energies and isotropic angular distributions. At lower bias frequencies (1–2 MHz), the extracted negative ions had energy in the range 2–25 eV and anisotropic angular distributions. Anisotropic negative ions, pointing perpendicular to the wafer surface, can be useful for neutralizing the positive charge accumulated at the bottom of micro-features due to the electron shading affect.

#### 4.5. Source pulsing with synchronous dc bias on a BE

Source pulsing with application of a synchronous bias (figure 18) on an auxiliary electrode (so-called BE) during a specified time window in the afterglow has been used to control the IED on the substrate electrode [32–34]. The advantage of this technique is that IEDs with controlled energy and narrow full-width at half-maximum (FWHM) may be obtained. As the plasma source power is turned OFF in the afterglow, the electron temperature (and plasma potential) plummets to  $<1 \text{ eV}$  within a few  $\mu\text{s}$  (figure 5). Thus, for a typical source

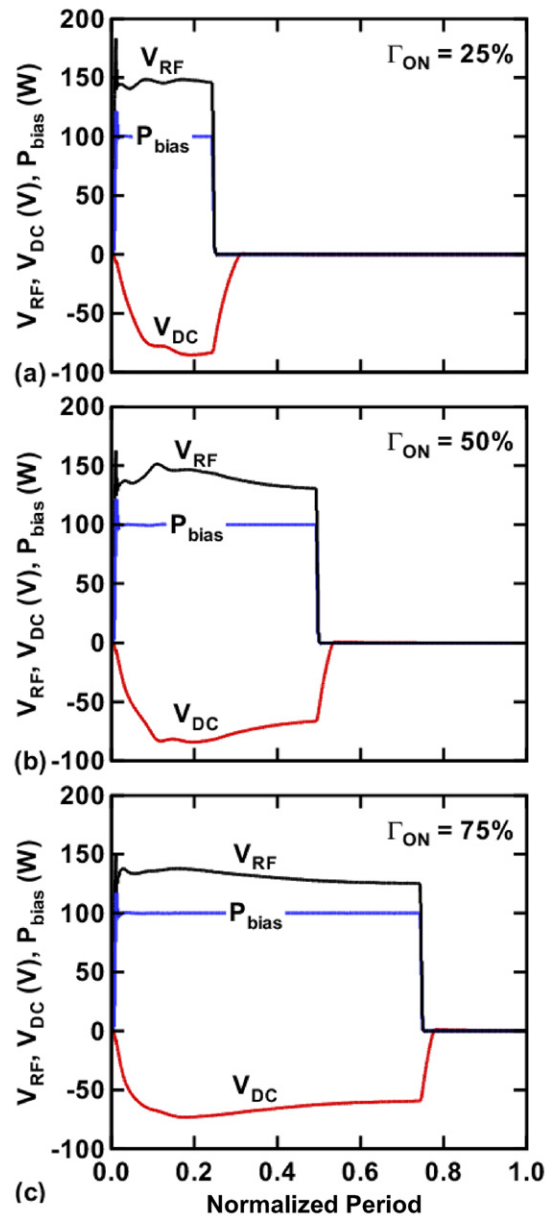
pulsing frequency of 10 kHz and a duty ratio of 50%, ( $50 \mu\text{s}$  active glow and  $50 \mu\text{s}$  afterglow), the electron temperature and plasma potential are, for the most part of the afterglow, at very low values. Under these conditions, application of a positive dc bias to a BE, raises the plasma potential by an amount controlled by the value of dc bias. That way, positive ions are expelled from the plasma, and assuming a collisionless sheath, bombard a grounded substrate with energy equal to the plasma potential. Furthermore, since the distribution of ion energies entering the sheath scales with  $T_e$  [96, 97], the FWHM of the IED on the substrate can be made very small ( $\sim 1 \text{ eV}$ ) by applying the dc bias late in the afterglow, when  $T_e$  is very low. Biasing in the afterglow has the additional advantage of better ion directionality on the substrate, since the IAD also depends on  $T_e$ . Assuming a Gaussian IAD, no collisions in the sheath, and a sheath potential  $V_{\text{sh}} \gg T_e$ , the IAD can be written as  $f(\theta) \approx C_N \exp(-\beta\theta^2)$  where  $C_N$  is a normalization factor and  $\beta = V_{\text{sh}}/T_+$ , with the ion temperature  $T_+$  expressed in V [98]. However, the ion temperature scales with  $T_e$  assuming that ions have their last collision in the presheath. Therefore, the ion flux becomes more anisotropic as  $T_e$  decreases in the afterglow making  $\beta$  larger.

Figure 19 shows measured IEDs on a grounded substrate in a pulsed ICP at different argon gas pressures. The ICP source power was modulated at 10 kHz and 20% duty ratio, i.e.



**Figure 16.** Ion energy-angular distributions (IEADs), averaged over the wafer, during each distinct phase of a pulse cycle of figure 14, for different duty ratios: (a) 25%, (b) 50% and (c) 75%. Synchronous biasing without phase difference under the following conditions: Ar/Cl<sub>2</sub> = 80/20, 10 mTorr, 100 sccm, 300 W peak ICP power, 100 W peak bias power and 5 kHz pulse frequency. Ramp-up and ramp-down duration was 2 μs each. IEADs are plotted using a log scale over 2 decades. From [94] with permission. Copyright 2009 AIP Publishing LLC.

20 μs ON and 80 μs OFF. A 24.4 V positive bias was applied synchronously to a BE for 50 μs during the afterglow (from t = 45 μs to t = 95 μs, the afterglow started at t = 20 μs).



**Figure 17.** Temporal dynamics of the RF bias voltage and self-generated dc bias voltage necessary to deposit the peak bias power (100 W) on the substrate electrode, for different duty ratios: (a) 25%, (b) 50% and (c) 75%. Synchronous biasing without phase difference under the following conditions: Ar/Cl<sub>2</sub> = 80/20, 10 mTorr, 100 sccm, 300 W peak ICP power, 100 W peak bias power, and 5 kHz pulse frequency. From [94] with permission. Copyright 2009 AIP Publishing LLC.

For a given pressure, the IED has two peaks. The broader peak at lower energies is due to the active glow and the part of the afterglow when there is no bias applied to the BE. The sharper peak at higher energies is due to the dc bias applied to the BE. It should be noted that since the substrate is grounded, the IED is a reflection of the plasma potential, assuming no ion-neutral collisions in the sheath. The location of the broader peak can be changed by changing pressure. As pressure increases, T<sub>e</sub> and the plasma potential both decrease. Thus the peak moves to lower energies. This is important if one desires to achieve a nearly monoenergetic IED on the substrate. The

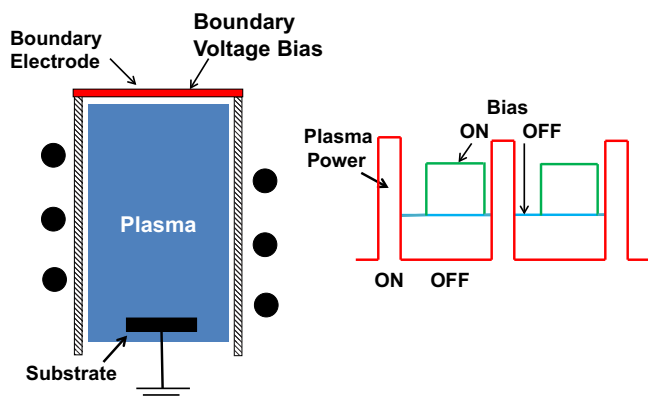


**Figure 18.** (a) Schematic of apparatus for generating nearly monoenergetic IEDs by utilizing synchronous pulsing. A dc pulse is applied on a BE in the afterglow of a pulsed discharge, to control the plasma potential. (b) Timing of power-modulated source plasma (red line) and synchronous dc pulse (green line) applied on BE.

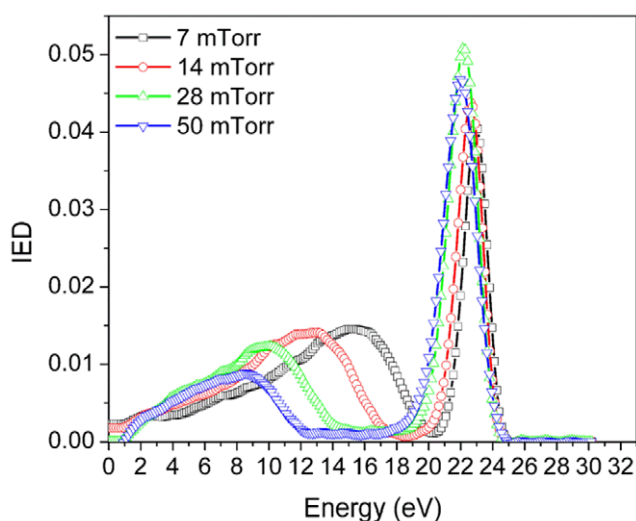


**Figure 19.** IEDs for different pressures under pulsed plasma conditions with a synchronous +24.4 V dc bias applied on the BE in the afterglow, over the time window,  $\Delta t_b = 45 - 95 \mu\text{s}$ . Other conditions: 10 kHz plasma power modulation frequency at 20% duty ratio, 120 W average power and 40 sccm argon gas flow. From [33] with permission.

lower peak of the IED has to lie entirely in the energy range of about <math>10\text{--}15\text{ eV}</math>, i.e. below the threshold for reactive ion etching (RIE). The sharper peak location can be adjusted by varying the dc bias applied to the BE. Thus, by varying pressure and/or dc bias the separation of the two peaks can be varied. The fraction of ions under each peak can also be adjusted by varying the duty ratio of the pulsed power or by varying the time window during which the bias is applied. Simulation results of IEDs obtained by applying synchronous bias in the afterglow of pulsed discharges and comparisons with data are given in [34, 99, 100].

The application of dc bias on an auxiliary electrode to control the plasma potential was implemented by Smith and Overzet [101], Coburn and Kay [102] and Panda *et al* [88]. A monoenergetic IED was obtained experimentally by Xu *et al* [32] by pulsing the source power of a CCP reactor (PRF =

5 kHz, duty ratio = 50%) and applying a dc bias on a BE during the afterglow of an argon plasma. An electrostatic filter was used to remove the low energy peak from the IED. Nam *et al* [100] employed PIC-MCC to simulate the system of Xu *et al*. Spatial gradients of the plasma potential were minimized in the afterglow allowing extraction of a monoenergetic, collimated ion beam. LP measurements indicated that the plasma potential was raised uniformly by applying a BE bias. The electron density and the EEDF were not affected when compared to the case of no bias applied. PIC-MCC simulations of the IEDFs were in excellent agreement with the experimental data. Diomede *et al* [103, 104] also conducted PIC-MCC simulations of the application of tailored dc voltage steps on an electrode. For the above methodology to work the auxiliary electrode should remain free of any insulating layers that may deposit on the electrode. Thus, this method will not be applicable to PECVD of insulating films (e.g.  $\text{SiO}_2$ )

#### 4.6. Control of the EEDF

The EEDF is critical for controlling the e-impact dissociation and ionization rates in a plasma, therefore controlling the radical and ion fluxes bombarding the substrate. In CW plasmas, the EEDF reaches a steady-state depending on externally controlled variables such as pressure and plasma excitation frequency [105, 106]. Pulsed plasmas offer flexibility in ‘shaping’ the EEDF to favor processes of interest. For example, lower PRF and smaller duty ratios produce larger excursions of the tail of the EEDF favouring large threshold e-impact processes (e.g. ionization or production of highly vibrationally excited hydrogen molecules [107]). On the other hand, during power OFF the EEDF cools down, favouring processes with low or no threshold (e.g. electron attachment to vibrationally excited hydrogen molecules to produce  $\text{H}^-$  or attachment to  $\text{Cl}_2$  to produce  $\text{Cl}^-$ ). Hopkins and Graham [84] used a LP to measure time-resolved electron energy probability functions (EEDFs) in a pulsed hydrogen discharge (source pulsing) sustained in a vessel with multipole magnetic confinement at a pressure of 2 mTorr. The magnetic poles were arranged to also form a magnetic filter separating the discharge in a ‘driver’ region and a downstream ‘extraction’ region. The purpose of the filter was to allow only cool electrons to pass into the extraction region where they could collide with vibrationally excited hydrogen molecules to produce  $\text{H}^-$  negative ions. The negative ions were extracted through an aperture in a biased plate forming one of the walls of the extraction region. The dc voltage applied to the filaments driving the discharge was pulsed ON for  $0 < t < 200 \mu\text{s}$  and OFF for  $200 \mu\text{s} < t < 2\text{ ms}$ . The EEDF was bi-Maxwellian in a CW discharge (for long active glow times) but became Maxwellian in the afterglow. It took  $\sim 160 \mu\text{s}$  to reach steady-state after power was turned ON. In the afterglow, diffusion cooling was the dominant loss of electron energy. Species loss was also generally controlled by diffusion to the walls of the discharge vessel.

Song and Kushner [107] simulated dual-frequency capacitively coupled reactors in Ar or  $\text{Ar}/\text{CF}_4/\text{O}_2$  (75/20/5) mixtures. The upper electrode was driven with 500 W (time-average power) at 40 MHz and could be pulsed. The lower

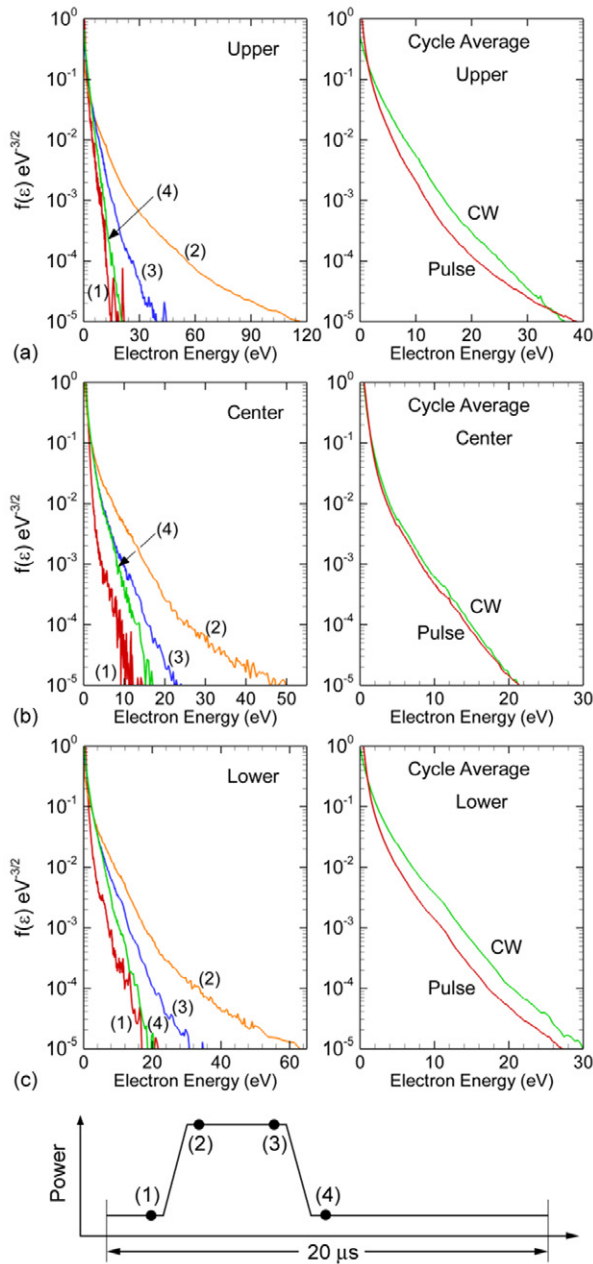


**Figure 20.** EEDFs in 40 mTorr Ar/CF<sub>4</sub>/O<sub>2</sub> = 75/20/5 dual-frequency capacitively coupled plasmas, at different times (1,2,3,4) during the pulse cycle, shown in the bottom figure. The lower frequency (10 MHz, 500 W) was applied in CW mode while the higher frequency (40 MHz, 500 W time-average) was pulsed (50 kHz PRF and 25% duty ratio). (a) Near the higher frequency sheath, (b) in the bulk plasma and (c) near the lower frequency sheath. Comparisons of the EEDF averaged over the pulse period with that obtained under CW excitation are shown in the right column. From [107] with permission.

(substrate) electrode was driven with 500 W of CW power at 10 MHz. Base case conditions were: 40 mTorr, 4 cm gap, 200 sccm flow rate, 50 kHz PRF and 25% duty ratio (*D*). Figure 20 shows the calculated EEDFs in the gas mixture at different times during the pulse (as shown in the schematic at the bottom figure) and at three locations in the interelectrode gap: (a) near the sheath edge of the upper electrode, (b) at the middle of the gap (in the bulk plasma), and (c) near the

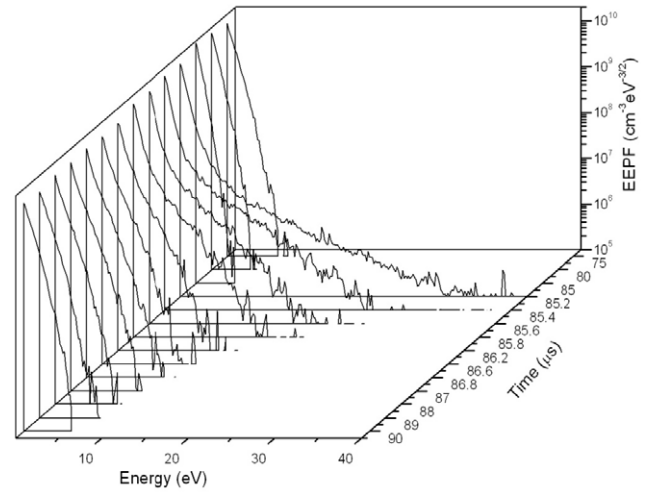


**Figure 21.** Time evolution of the calculated EEPF at the discharge centre. Power to a 10 mTorr Ar CCP was modulated at 10 kHz with duty ratio 50% (50 μs active glow and 50 μs afterglow). A 50 V dc bias was applied 20 μs into the afterglow (at *t* = 70 μs), followed by a 300 V dc bias applied at *t* = 85 μs until the end of the afterglow (*t* = 100 μs). Time *t* = 0 refers to the start of the active glow (plasma ON). The EEPF is heated at the time the 300 V dc bias pulse is applied. A Maxwellian distribution would be a straight line on this plot. From [103] with permission. Copyright AIP Publishing LLC.

sheath edge of the lower electrode. Comparisons of the cycle average EEDFs (at the same time-average power) with the EEDFs under CW power on both electrodes are also shown in figure 20. The tail of the EEDF is modulated violently within a pulse. The tail extends furthest into high energies when the power has reached its peak value (time 2). This effect can be exacerbated by using low PRF and low *D*. Low PRF implies that the electron density decreases to very low values during the long afterglow. Consequently, the excursion of the electric field to ignite the plasma during power turn ON will be more severe. This corresponds to the electron temperature spike during the early active glow; the lower the electron density at the end of the preceding afterglow, the stronger the spike. The tail of the EEDF near the upper electrode sheath extends to higher energies (compared to that near the lower sheath) due to more efficient heating by the high frequency oscillations of the upper sheath (heating scales with  $\omega^2$ , see [1, p 410]). Also the lower EEDF has hotter electrons compared to that at the centre due to heating by the oscillating sheath of the lower electrode. The pulse period averaged (PPA) EEDF is very similar to that under CW conditions. However, the PPA EEDF misses the violent excursions of the tail of the distribution that have direct bearing on very high threshold reactions, which are inaccessible by the CW EEDF.

The effect of a dc bias on the plasma dynamics of a power-modulated CCP reactor was simulated by Diomede *et al* [103]. The PRF was 10 kHz and the duty ratio was 50% (50 μs active glow and 50 μs afterglow, *t* = 0 corresponds to the start of the active glow). A ‘staircase’ dc voltage was applied to the powered electrode, when the source power was OFF (during the afterglow). Specifically, 50 V dc bias was applied 20 μs into the afterglow (at *t* = 70 μs) for 15 μs, followed by a 300 V dc bias applied at *t* = 85 μs until the end of the pulse (*t* = 100 μs). The calculated time-resolved

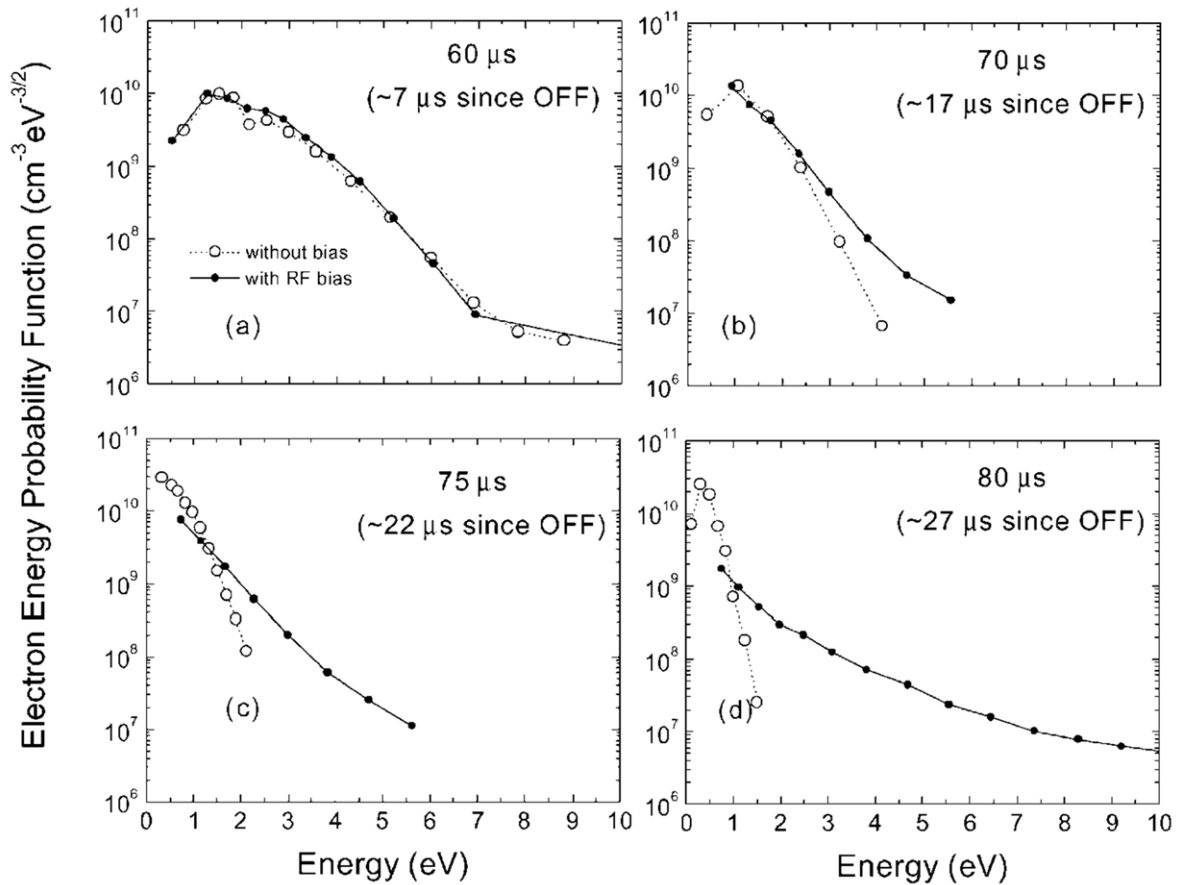


**Figure 22.** EEPFs for different times (around the transition to the ‘RIE mode’) during the afterglow of a 10 mTorr  $\text{Cl}_2$  plasma. The source power (300 W net, time-averaged), was modulated  $50 \mu\text{s}$  ON/ $50 \mu\text{s}$  OFF. Open symbols denote the case with no bias; closed symbols denote the case with RF bias (70 W) on the substrate electrode. A Maxwellian distribution would be a straight line on this plot. From [51] with permission.

EEPFs around the time the 300 V dc was applied are shown in figure 21. In this plot, a Maxwellian EEPF will be a straight line with slope proportional to  $1/T_e$ . The application of 300 V dc modifies the EEPF from bi-Maxwellian with a cold tail to a bi-Maxwellian with a hot tail. The EEPF is heated during the ramp-up of the dc bias by the expanding sheath. Electron heating of the tail of the EEPF over this short transient, however, hardly affected the electron density evolution. There was a perceptible but not as significant change in the EEPF immediately following the application of 50 V dc as well (not shown). In contrast, by periodically applying a much stronger negative dc pulse ( $-2500$  V) to the powered electrode of an otherwise conventional CCP, Sun *et al* [108] observed not only heating of the EEDF but also an increase in plasma density.

Malyshev and Donnelly [51] presented an experimental study of the dynamics of an ICP in 10 mTorr chlorine (100 sccm), under source pulsing (300 W net average power, PRF 10 kHz, duty ratio 50%), and with CW bias (70–100 W at 12.5 MHz) on the substrate electrode. They used a LP to measure electron and positive-ion densities, as well as the time-resolved EEPF. Without bias power (reference case), the electron temperature exhibited the expected behaviour; it overshoot upon power turn ON, then reached a quasi-steady state at about 2.5 eV for the remainder of the  $50 \mu\text{s}$ -long active glow. Upon power turn OFF,  $T_e$  dropped initially quickly and

then more gradually to reach a very low value ( $\sim 0.25$  eV) at the end of the  $50 \mu\text{s}$ -long afterglow. When the CW bias power was applied,  $T_e$  showed the same behaviour, as without bias, for the duration of the active glow, and the subsequent  $25 \mu\text{s}$  into the afterglow. At that point,  $T_e$  started to increase, reaching almost 7 eV at the end of the afterglow. This re-heating of the electron energy distribution was attributed to stochastic heating by the oscillating sheath of the biased electrode. Meanwhile, neither the electron nor the positive-ion density was affected by the bias; both continued to decay throughout the  $50 \mu\text{s}$  afterglow, as they did without bias. However, when the afterglow was made sufficiently long, the plasma density started to increase as the system transitioned to a so-called ‘reactive ion etching mode’, sustained solely by the bias power. This transition occurred when the positive-ion density in the afterglow reached the value corresponding to a capacitively coupled plasma at the applied bias power and in the absence of source power. Time-resolved EEPFs in the afterglow, with and without applied CW bias, are shown in figure 22 which depicts the transition to the RIE mode when a bias is applied.  $7 \mu\text{s}$  into the afterglow, bias has no influence on the EEPF. However,  $17 \mu\text{s}$  into the afterglow, the EEPF with bias is ‘hotter’ (not as steep), compared to that without bias. The difference between the two EEPFs becomes larger as time progresses; the EEPF without bias keeps cooling down, while

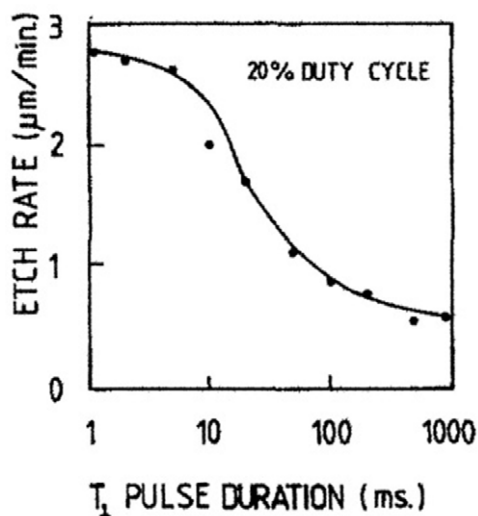


**Figure 23.** Etch rate of silicon in  $\text{SF}_6$  pulsed plasma for different pulse durations and a duty ratio of  $D = 20\%$ . For very short pulse durations (compared to the F-atom lifetime), the CW plasma etch rate  $R_{\text{CW}}$  is obtained. For very long pulse durations, the etch rate is  $D \times R_{\text{CW}}$ . From [21] with permission. Copyright 1987 AIP Publishing LLC.

that with bias keeps heating up. Figure 22(d) shows that the EEPF with bias has a bi-Maxwellian character typical of sheath heating in CCPs [105, 109].

## 5. Applications of pulsed plasmas

### 5.1. Etching of Si-based materials

Very high etch rate ( $\sim 3 \mu\text{m min}^{-1}$ ) of silicon in  $\text{SF}_6$  plasma sustained by a resonant RF source was observed by Boswell and Henry [110]. By pulsing the plasma (source pulsing), the selectivity of etching Si versus  $\text{SiO}_2$  could be varied between 100 at high repetition rates, to 6 at low repetition rates or CW plasma. When the substrate was biased, the etch profile varied from isotropic at high repetition rates to anisotropic at CW operation. Using the same apparatus, Boswell and Porteous found the Si etch rate to be essentially the same in CW plasma and in pulsed plasma with short pulses ( $\sim 1$  ms period) at a duty ratio of only 20%. This was attributed to etching by F atoms during the afterglow. The F-atom lifetime in the afterglow was determined to be  $\sim 50$  ms. Therefore for short (e.g. 1 ms) pulses (corresponding to short afterglow duration), the F-atom density would be at the level of CW plasma. For long (e.g. 1000 ms) pulses, the F atoms density would be near zero for almost all of the afterglow. In this case the etch rate would be that of CW plasma multiplied by the duty ratio (figure 23). Analytical expressions for the space-averaged (well-mixed reactor or global model) reactant concentration and reaction rate as a function of the relevant parameters were given by Park and Economou for PECVD (appendix B [27]). The same model can be readily adapted to etching, assuming that ion-assisted etching does not play a role (chemical etching only).

Samukawa [43] etched Si with chlorine in an ECR reactor at 2 mTorr. The source power was pulsed (PRF 10–100  $\mu\text{s}$ , 50% duty ratio) while the substrate electrode was biased

with 600 kHz RF power. Enhancement in etch rate and suppression of notching was thought to be the result of alternating bombardment of the substrate with positive and negative ions under the influence of the low RF frequency. In other studies [111] source pulsing was used to control the  $\text{F}/\text{CF}_2$  radical density ratio in a  $\text{CHF}_3$  plasma. Low values of this ratio are required for selective etching of  $\text{SiO}_2$  over Si.

Shin and co-workers [20] did experiments on etching of  $\text{SiO}_2$  in  $\text{C}_4\text{F}_8/\text{Ar}$  ICPs by pulsing both the source and bias power (synchronous pulsing), varying the phase between them. They observed heavy polymerization in the out-of-phase condition, which enhanced selectivity of  $\text{SiO}_2$  etching compared to the photoresist mask. Polymer deposition was attributed to ion-enhanced polymerization due to the higher  $\text{CF}_x^+$  ( $x = 1, 2, 3$ ) ion energies (10s of eV) in the out-of-phase condition, measured with a mass spectrometer equipped with an ion energy analyser. Using optical emission spectroscopy, they also observed higher concentration of  $\text{C}_2$  in the out-of-phase condition, and surmised that  $\text{C}_2$  was another contributor to polymer deposition.

Petit-Etienne *et al* [17] studied experimentally silicon recess as a result of the overetch step in gate etching using  $\text{HBr}/\text{O}_2/\text{Ar}$  (200/5/150 sccm) plasmas at 50 mTorr. Such undesirable Si loss occurs in the active region of the transistor due to oxidation of the crystalline Si underneath a thin gate oxide. The oxidized silicon layer is inevitably removed by the wet cleaning step following etching. It was found that pulsing (5 kHz, 20% duty ratio) the plasma source (500 W peak power) synchronously (no phase delay) with the bias power (100 W peak) reduced the damaged layer thickness to 0.8 nm, compared to 4 nm in the CW mode. It has been theorized that Si oxidation through a thin gate oxide during gate etching occurs in a synergistic manner. Protons ( $\text{H}^+$ ), generated in the plasma, create diffusion paths through the gate oxide, leading to partial amorphization of the silicon surface under the oxide. Species (especially Br) diffusing or implanting through the gate oxide react with the modified silicon layer to form  $\text{SiBr}_x$ , which in turn is readily oxidized by oxygen in the plasma or moisture during exposure to ambient air. Pulsing the plasma reduces the gas dissociation, preserving the molecular nature of the reactants in the feedstock gas. Molecular ions acquire the same energy in the sheath as atomic ions but, upon impact, molecular ions break apart in atoms each carrying a fraction of the original ion energy. This creates less ion induced damage and reduces the diffusion rate of species through the thin gate oxide, thus reducing the thickness of the damaged silicon underlayer. In a more recent study, Petit-Etienne *et al* [112] investigated etching of silicon using 20 mTorr  $\text{Cl}_2$  in an ICP without substrate bias. By pulsing the plasma source power (1 kHz, 10% duty ratio) they were able to control Si etching down to  $0.2 \text{ nm min}^{-1}$ . *In situ* angle resolved XPS of the etched samples revealed that the Si surface was less chlorinated, the top damaged layer was thinner and wall sputtering was reduced in the pulsed plasma compared to CW plasma. Control of etch rate with monolayer accuracy is important for atomic layer etching (ALET) [113–115].

The conventional thinking is that differential charging is mitigated in pulsed electronegative plasmas by negative

ions extracted from the plasma. Hwang and Giapis [116] proposed a different mechanism for charging damage reduction in pulsed discharges, based on the fact that low energy positive ions are created in the afterglow, due to the decay of the sheath electric field. The trajectory of these ions is more amenable to deflection by the local electric fields at the micro-feature entrance, where the ions can neutralize (at least partly) the negative charge accumulated in that region due to the *electron shading* effect. At the same time, current balance at the micro-feature bottom is satisfied at lower charging potential, making notching and gate oxide degradation less prevalent. Directional injection of negative charges (electrons and negative ions) by applying a positive substrate bias in the afterglow would also help in neutralizing the accumulated positive charge at the bottom of the feature.

Ishikawa *et al* [117] studied UV photon-induced defects (such as E' centres) in silicon dioxide exposed to a plasma. The defect density was reduced when using a pulsed plasma, as compared to a CW plasma. This was attributed to lower dose of UV exposure in the pulsed plasma since the electrons cool rapidly in the afterglow and production of UV radiation ceases within a few  $\mu\text{s}$  after the plasma is turned OFF. In addition, defects introduced in the pulsed plasma could be annealed at a lower temperature compared to those created in a CW plasma.

Shibayama *et al* [16] etched Si in a pulsed SF<sub>6</sub> microwave plasma while applying a 400 kHz CW bias on the substrate electrode. Ions emanating from the plasma were characterized by a quadrupole mass spectrometer. The dominant negative ion was found to be F<sup>-</sup>. The Si etch rate as a function of pressure followed the same trend with the F<sup>-</sup> density; both attained their maximum value at 40 mTorr. It was surmised that the low frequency bias extracted negative ions (as well as positive ions) out of the plasma, and that negative ions were more effective at etching Si compared to positive ions. However, more direct evidence is required to support this proposition.

Subramonium and Kushner [28] simulated the effect of plasma source pulsing on reducing non-uniformities in an ICP. Azimuthal asymmetry in the ion density profiles in the CW plasma was due to the presence of a pump port opening in the wall, extending over a 60° arc in one side of the reactor. The absence of a wall reduced the surface recombination loss of positive ions, and resulted in a local enhancement of the ion concentration (figure 24). Pulsing the plasma power could alleviate these concentration gradients, by allowing the ions to diffuse (ambipolar diffusion) during the afterglow of the pulsed plasma, when ion production had ceased, thereby reducing the concentration gradients. For given PRF, a lower duty ratio, hence longer afterglow time, gave better azimuthal uniformity because the homogenizing effect of diffusion operated for longer time. The azimuthal non-uniformities are not pronounced right underneath the dielectric window (left column in figure 24) because the pump opening is restricted to the lower part of the cylindrical wall.

Ono and Tuda [118] simulated the profile evolution of 2D trenches etched in silicon in a high density chlorine plasma, under pulsed plasma conditions. The time-dependent chlorine surface coverage was found using a Langmuir–Hinshelwood model. Their study focused in the ‘neutral starved’ regime

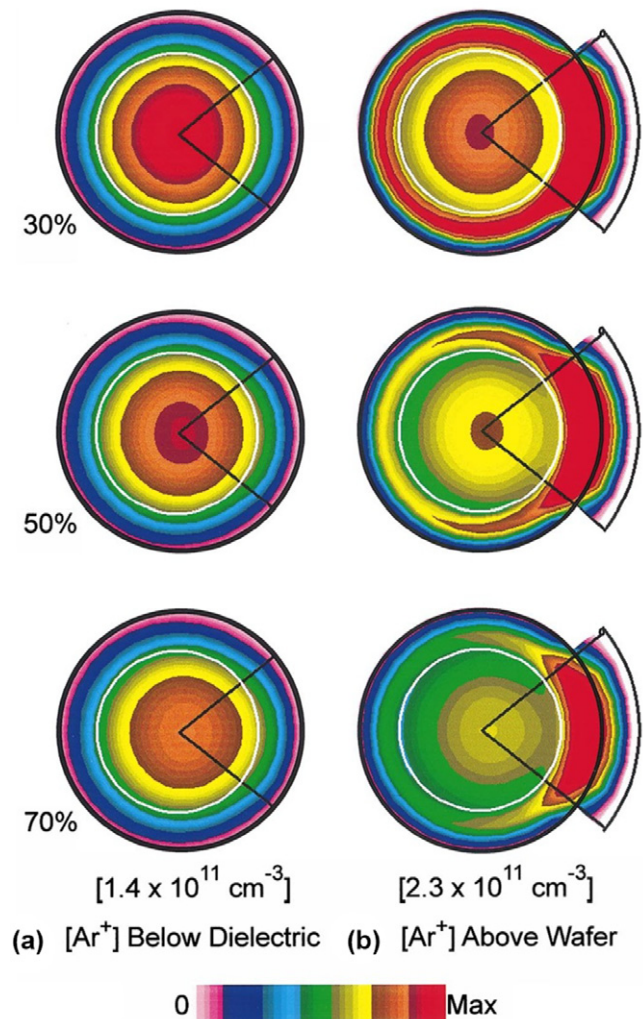


**Figure 24.** Argon ion density averaged over the pulse period at the end of the sixth pulse (source pulsing) following CW operation, for duty ratios of 30%, 50% and 70%. (a) Just below the dielectric of the ICP with stove-top coil; (b) just above the wafer. Other conditions: 10 mTorr, 50 sccm Ar, 250 W time-average power, PRF 10 kHz. Values in brackets indicate the maximum value of ion density for each column. From [28] with permission. Copyright 2004 AIP Publishing LLC.

(neutral-to-ion flux ratio of 3) at low pressure (1 mTorr). Figure 25 shows the profile evolution of trenches with different aspect ratios. ARDE is clearly observed. Under their conditions, a period of 10 ms with 10% duty ratio resulted in the least ARDE. This was explained based on the Cl surface coverage at the bottom of the trench being highest under these conditions.

Schaepkens *et al* [119] presented experiments on the effect of RF bias pulsing (CW source power) on the rate and selectivity of SiO<sub>2</sub> etching in fluorocarbon plasmas. For the blanket films examined, the oxide etching rate, as a function of self-bias voltage, depended on duty ratio but not on pulsing period (1–900 ms). The etching rate of silicon and photoresist displayed the same behaviour with respect to self-bias voltage. It was concluded that pulsing the RF bias did not offer any selectivity advantages compared to CW plasma. Raballand *et al* [120] studied etching of SiOCH (a low-*k* dielectric), SiCH (an etch stop layer) and SiO<sub>2</sub> (a masking layer) in CHF<sub>3</sub> ICP with pulsed bias (1500 W source power, 40 sccm flow and

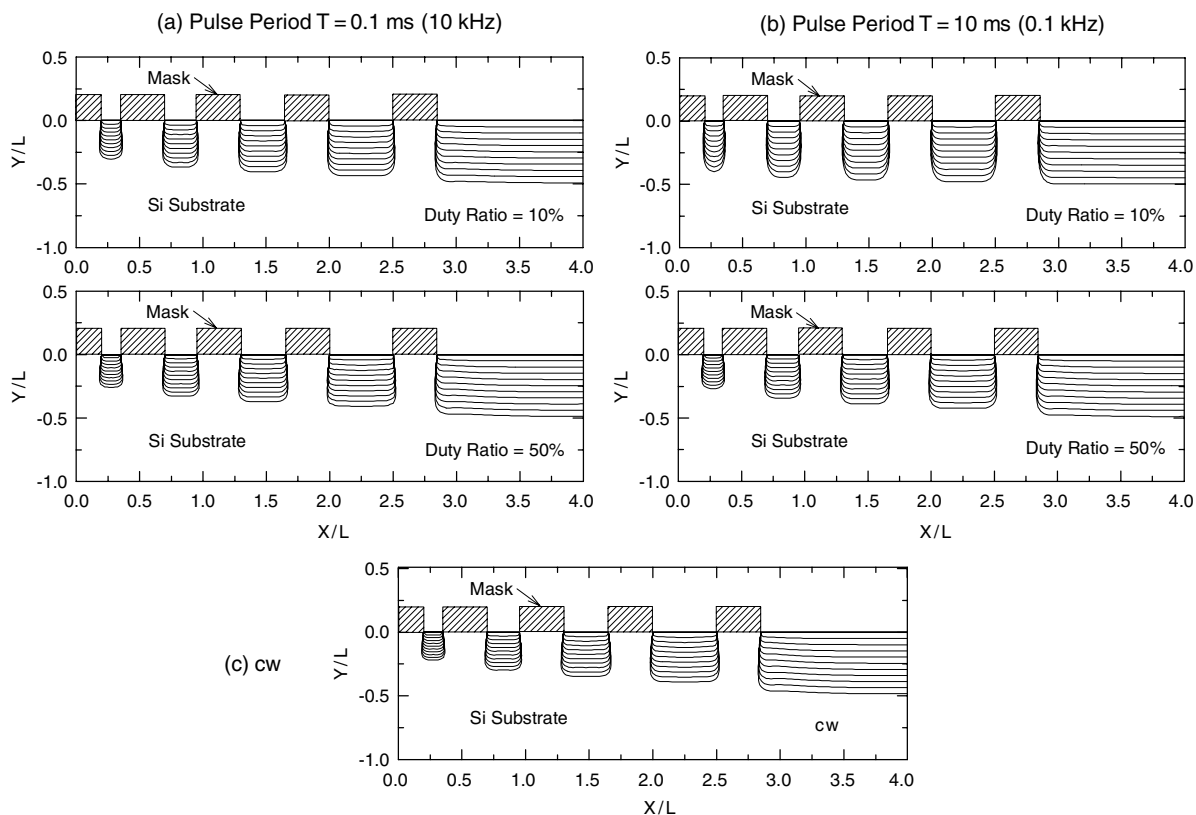


**Figure 25.** Simulated profile evolution of long rectangular trenches etched in silicon with chlorine plasma. (a) Pulsed plasma with pulsing period of 0.1 ms and duty ratio 10% (top) and 50% (bottom). (b) Pulsed plasma with pulsing period of 10 ms and duty ratio 10% (top) and 50% (bottom). (c) CW plasma. Other conditions: pressure = 1 mTorr, CW ion flux  $10 \text{ mA cm}^{-2}$  and CW neutral-to-ion flux ratio = 3. A period of 10 ms with 10% duty ratio results in the least ARDE. From [118] with permission. Copyright 2000 Elsevier.

5 mTorr pressure). In accordance with Schaeckens *et al* [119], they observed that the etching rate of porous SiOCH was independent of PRF, in the range 1 Hz to 10 kHz investigated, but depended on duty ratio. Etching selectivity of porous SiOCH versus SiCH and SiO<sub>2</sub> was considerably increased when the duty ratio was decreased.

Banna *et al* [121] reported a combined experimental-simulation study of conductor (poly-Si gate) etching using a pulsed ICP with synchronous pulsed substrate bias. By varying the pulsed plasma parameters (pulse frequency, duty cycle, phase difference between the source and bias pulsing), they demonstrated that synchronous pulsing can be used to control the etching uniformity, selectivity, and feature profile. In addition, there was significant reduction of the electron shading effect and the plasma induced damage. Finally, it was possible to independently control the ion flux and energy bombarding the substrate.

Besides etching, pulsed plasmas have also been used in plasma enhanced chemical vapour deposition (PECVD) in an effort to tailor the deposited film microstructure and resulting properties [122–124].

### 5.2. Emerging applications

Pulsed plasmas may find application in the burgeoning field of ALET, where the goal is to etch a solid with atomic layer precision [125]. Conventional ALET consists of four steps

[114]: (1) chemisorption of a reactive gas to form a monolayer of the gas on the solid surface; (2) evacuation of the chamber to avoid unwanted etching with background etchant; (3) exposure of the chemisorbed layer to a monoenergetic ion (or fast neutral) beam to remove the top layer of the solid (attached to the chemisorbed gas). An ion beam is extracted from a plasma; a neutral beam is formed by neutralizing ions extracted from a plasma. (4) Evacuation of the reaction products. In ideal ALET, each cycle removes exactly one monolayer of a crystalline solid. The cycle can be repeated as many times as the number of monolayers to be removed [113, 126–128]

There are two issues with traditional ALET. First, gas pulsing is a disadvantage, exacerbated by the fact that etching gases such as Cl<sub>2</sub> have a long residence time on the chamber walls, requiring long pumping periods before the inert gas plasma is ignited to execute step (3) above. This makes the etching rate slow, even for very thin films. Second, the etching rate per cycle may not necessarily remain constant. Ion bombardment induced roughening, for example, can cause the saturated layer thickness to increase with cycle number, and hence lead to an increase in etching rate with cycle number, losing atomic layer precision.

A new methodology for rapid ALET has been presented [115]. First, a CW RF ICP is ignited in dilute (e.g. 1%) Cl<sub>2</sub>/Ar gas for approximately 1 s, to provide reactants (e.g. Cl) to form a chemisorbed layer (e.g. SiCl<sub>x</sub>) on the Si surface. During this time, the ion bombardment energy is too low ( $\sim 10 \text{ eV}$ ) for any

etching to occur. Next, a pulsed ICP, lasting typically a total of  $\sim 0.5$  s, is used to remove the chemisorbed layer. During the 0.5 s interval, the plasma is pulsed ON and OFF. For most of the 100  $\mu$ s afterglow (OFF) period, a positive dc voltage is applied to a BE raising the plasma potential and expelling positive ions (with a nearly monoenergetic IED), out of the plasma to the grounded substrate [33]. Control of the IED is critical to effect chemical sputtering of the chemisorbed halogenated layer, without physical sputtering of the underlying substrate (self-limiting process). This extreme selectivity requires very narrow IED, so that ALET with monolayer accuracy may be achieved. The cycle of 1 s surface chlorination, followed by 0.5 s product removal, may be repeated as many times as necessary to remove the desired number of atomic layers off of the substrate.

Charging damage of sensitive devices may be minimized or totally eliminated by using energetic neutrals (10s to 100s eV) to perform the action of ions and turn 'reactive ion etching' into 'neutral beam etching' [129]. A promising method to generate a fast neutral beam is to extract ions from a plasma, under the influence of bias, and neutralize these ions by grazing angle collisions on the internal walls of high aspect ratio (e.g. 10:1) holes of a grid. Due to the grazing angle collision only a small fraction of the initial energy of the parent ion is lost. Depending on the kind of fast neutrals desired, a pulsed plasma in an appropriate electronegative gas (for example  $\text{Cl}_2$  or  $\text{SF}_6$  to generate Cl or F atoms, respectively) may be used and a negative potential applied to a BE (or a positive potential applied to the extraction grid) during the afterglow, to force negative ions out of the plasma and through the grid holes. Application of a negative dc bias to a BE late enough in the afterglow when the plasma potential has dropped to very low value, can result in a nearly monoenergetic ion flux entering the grid holes. The energy distribution of the outcoming neutral beam is expected to be broader [130], but it may still be tight enough to achieve selective etching.

### 5.3. Power delivery

Power delivery is one of the challenges for efficient utilization and reproducibility of pulsed plasmas. In particular, mechanical matching networks used in plasma reactors cannot follow the variation of plasma impedance over pulsing time scales of 10–100s of  $\mu$ s. Several methods have been proposed to alleviate this problem [121, 131]. (a) The matching network is pre-set to match the impedance of the CW plasma. This method should work best if, after the power is turned ON, the plasma reaches a quasi-steady state quickly, and this steady state is the same as for a CW plasma at a power equal to the peak power of the pulsed plasma. This is the case for noble gas plasmas [46, 58], but it does not hold for reactive gas plasmas. (b) The applied excitation frequency is tuned 'on the fly' in an effort to match the load impedance as it varies with time. Frequency tuning is done electronically so it can respond to the pulsing time scale, and (c) a combination of (a) and (b). The power reported in the literature is often a nominal value and not necessarily the power dissipated in the plasma. Even when the net (forward minus reflected) power is given, there

could be a significant fraction of power dissipated as Ohmic losses (e.g.  $I^2R$  loss in the inductive coil) which often times is not accounted for.

In many cases (especially in laboratory plasma reactors) capacitive coupling is blocked (for example ICP with Faraday shield) to obtain a quiescent plasma potential. Suppressing plasma potential oscillations due to capacitive coupling may be necessary to achieve nearly monoenergetic IEDs. However, when such systems are operated in pulsed plasma mode, especially with attaching gases, and with a relatively long afterglow duration, electrons may essentially disappear by the end of the afterglow. The absence of electrons, and the lack of capacitive coupling, make re-ignition of the plasma, when power is turned back ON, very challenging. An auxiliary (igniter) plasma, operated in CW mode in communication with the main plasma, could provide enough seed electrons to re-ignite the main plasma [132].

## 6. Concluding remarks

Power-modulated (pulsed) plasmas hold promise in resolving some of the challenges of manufacturing nano-devices with sub-10 nm design rules. The choice of the kind of pulsing (source, bias, synchronous or other), and judicious selection of the pulsing frequency(ies) and duty ratio(s) open new processing windows with unprecedented flexibility. For example, the electron and ion distribution functions can be tailored to independently control the radical and ion fluxes, as well as the ion energy, to better satisfy process requirements. Application of power at multiple frequencies (for example dual-frequency [93, 107] or even triple frequency capacitively coupled plasmas) and the possibility of pulsing the power at each of these frequencies, introduces a herculean problem in terms of process design and optimization. Another possibility is to use dc pulsing or RF/dc hybrids to better tailor the IED and the EEDF simultaneously [104, 108]. The problem of the plethora of knobs is exacerbated by the need to match the different pulsed powers to the plasma. The inclusion of dc bias does not present power matching problems, but may result in charging of insulated wafers. Such methodologies, yet to be applied to manufacturing, can provide enormous flexibility in trying to satisfy the often contradictory process requirements.

## Acknowledgments

Financial support for this work was provided by the Department of Energy, Office of Fusion Energy Science, contract DE-SC0001939, and the National Science Foundation grants CMMI-1030620, and IIP-1343387.

## References

- [1] Lieberman M A and Lichtenberg A J 2005 *Principles of Plasma Discharges and Materials Processing* 2nd edn (New York: Wiley-Interscience)
- [2] Franz G 2009 *Low Pressure Plasmas and Microstructuring Technology* (Berlin: Springer)

- [3] Kong M G, Kroesen G, Morfill G, Nosenko T, Shimizu T, van Dijk J and Zimmermann J L 2009 Plasma medicine: an introductory review *New J. Phys.* **11** 115012
- [4] Cheung K P 2001 *Plasma Charging Damage* (London: Springer)
- [5] Shin H, Zhu W, Economou D J and Donnelly V M 2012 Surprising importance of photo-assisted etching of silicon in chlorine-containing plasmas *J. Vac. Sci. Technol. A* **30** 021306
- [6] Cheung K P and Chang C P 1994 Plasma-charging damage: a physical model *J. Appl. Phys.* **75** 4415
- [7] Arnold J C and Sawin H H 1991 Charging of pattern features during plasma etching *J. Appl. Phys.* **70** 5314
- [8] Economou D J and Alkire R C 1988 Effect of potential field on ion deflection and shape evolution of trenches during plasma-assisted etching *J. Electrochem. Soc.* **135** 941
- [9] Kinoshita T, Hane M and McVittie J 1996 Notching as an example of charging in uniform high density plasmas *J. Vac. Sci. Technol. B* **14** 560
- [10] Hwang G S and Giapis K P 1997 On the origin of the notching effect during etching in uniform high density plasmas *J. Vac. Sci. Technol. B* **15** 70
- [11] Watanabe M, Shaw D M and Collins G J 2001 Reduction of microtrenching and island formation in oxide plasma etching by employing electron beam charge neutralization *Appl. Phys. Lett.* **79** 2698
- [12] Gottscho R A, Jurgensen C W and Vitkavage D J 1992 Microscopic uniformity in plasma etching *J. Vac. Sci. Technol. B* **10** 2133
- [13] Samukawa S and Mieno T 1996 Pulse-time modulated plasma discharge for highly selective, highly anisotropic and charge-free etching *Plasma Sources Sci. Technol.* **5** 132
- [14] Samukawa S, Ohtake H and Mieno T 1996 Pulse-time-modulated electron cyclotron resonance plasma discharge for highly selective, highly anisotropic, and charge-free etching *J. Vac. Sci. Technol. A* **14** 3049
- [15] Samukawa S 1994 Pulse-time-modulated electron cyclotron resonance plasma etching for highly selective, highly anisotropic, and notch-free polycrystalline silicon patterning *Appl. Phys. Lett.* **64** 3398
- [16] Shibayama T, Shindo H and Horiike Y 1996 Silicon etching by alternating irradiations of negative and positive ions *Plasma Sources Sci. Technol.* **5** 254
- [17] Petit-Etienne C, Darnon M, Vallier L, Pargon E, Cunge G, Boulard F, Joubert O, Banna S and Lill T 2010 Reducing damage to the Si substrate during gate etching processes by synchronous plasma pulsing *J. Vac. Sci. Technol. B* **28** 926
- [18] Sugai H, Nakamura K, Hikosaka Y and Nakamura M 1995 Diagnostics and control of radicals in an inductively coupled etching reactor *J. Vac. Sci. Technol. A* **13** 887
- [19] Samukawa S 1993 Time-modulated electron cyclotron resonance discharge for controlling the polymerization in SiO<sub>2</sub> etching *Japan. J. Appl. Phys.* **32** 6080
- [20] Shin K S, Shi K K, Kang C J, Jung C, Jung C O, Moon J T and Lee M Y 1998 Enhancement of mask selectivity in SiO<sub>2</sub> etching with a phase-controlled pulsed inductively couple plasma *Japan. J. Appl. Phys.* **37** 2349
- [21] Boswell R W and Porteous R K 1987 Etching in a pulsed plasma *J. Appl. Phys.* **62** 3123
- [22] Jiang P, Economou D J and Shin C B 1995 Effect of power modulation on radical concentration and uniformity in a single-wafer plasma reactor *Plasma Chem. Plasma Process.* **15** 383
- [23] Verdeyen J, Beberman J and Overzet L 1990 Modulated discharges: effect on plasma parameters and deposition *J. Vac. Sci. Technol. A* **8** 1851
- [24] Bouchoule A and Ranson P 1991 Study of volume and surface processes in low pressure radio frequency plasma reactors by pulsed excitation methods: I. Hydrogen–argon plasma *J. Vac. Sci. Technol. A* **9** 317
- [25] Bouchoule A, Plain A, Boufendi L, Blondeau J Ph and Laure C 1991 Particle generation and behavior in a silane–argon low-pressure discharge under continuous or pulsed radio-frequency excitation *J. Appl. Phys.* **70** 1991
- [26] Watanabe Y, Shiratani M and Makino H 1990 Powder-free plasma chemical vapor deposition of hydrogenated amorphous silicon with high rf power density using modulated rf discharge *Appl. Phys. Lett.* **57** 1616
- [27] Park S-K and Economou D J 1991 Analysis of a pulsed-plasma chemical vapor deposition reactor with recycle *J. Electrochem. Soc.* **138** 1499
- [28] Subramonium P and Kushner M J 2004 Pulsed plasmas as a method to improve uniformity during materials processing *J. Appl. Phys.* **96** 82
- [29] Banna S, Agarwal A, Cunge G, Darnon M, Pargon E and Joubert O 2012 Pulsed high-density plasma for advanced dry etching processes *J. Vac. Sci. Technol. A* **30** 040801
- [30] Tserepi A D, Dunlop J R, Preppernau B L and Miller T A 1992 Effect of surfaces on H-atom concentration in pulsed and continuous discharges *J. Vac. Sci. Technol. A* **10** 1188
- [31] Kiss L D B and Sawin H H 1992 Comparison of CF<sub>3</sub>Cl and C<sub>2</sub>F<sub>6</sub> + Cl<sub>2</sub> plasma chemistry by power modulation *J. Electrochem. Soc.* **139** 1414
- [32] Xu L, Economou D J, Donnelly V M and Ruchhoeft P 2005 Extraction of a nearly monoenergetic ion beam from a pulsed plasma *Appl. Phys. Lett.* **87** 041502
- [33] Shin H, Zhu W, Xu L, Ouk T, Economou D J and Donnelly V M 2011 Control of ion energy distributions using a pulsed plasma with synchronous bias on a boundary electrode *Plasma Sources Sci. Technol.* **20** 055001
- [34] Logue M D, Shin H, Zhu W, Xu L, Donnelly V M, Economou D J and Kushner M J 2012 Ion energy distributions in inductively coupled plasmas having a biased boundary electrode *Plasma Sources Sci. Technol.* **21** 065009
- [35] Lafleur T and Booth J P 2012 Control of the ion flux and ion energy in CCP discharges using non-sinusoidal voltage waveforms *J. Phys. D: Appl. Phys.* **45** 395203
- [36] Lampe M, Manheimer W M, Fernsler R F, Slinker S P and Joyce G 2004 The physical and mathematical basis of stratification in electronegative plasmas *Plasma Sources Sci. Technol.* **13** 15
- [37] Daniels P G, Franklin R N and Snell J 1990 The contracted positive column in electronegative gases *J. Phys. D: Appl. Phys.* **23** 823
- [38] Tsendin L D 1989 Plasma stratification in a discharge in an electronegative gas *Sov. Phys.—Tech. Phys.* **34** 11
- [39] Kaganovich I D, Franklin R N and Demidov V I 2010 Principles of transport in multicomponent plasmas *Introduction to Complex Plasmas* ed M Bonitz *et al* (Berlin: Springer) pp 17–39
- [40] Kouznetsov I G, Lichtenberg A J and Lieberman M A 1999 Internal sheaths in electronegative discharges *J. Appl. Phys.* **86** 4142
- [41] Kolobov V I and Economou D J 1998 Ion–ion plasmas and double layer formation in weakly collisional electronegative discharges *Appl. Phys. Lett.* **72** 656
- [42] Kono A 1999 Formation of an oscillatory potential structure at the plasma boundary in electronegative plasmas *J. Phys. D: Appl. Phys.* **32** 1357
- [43] Samukawa S 1996 Pulse-time-modulated electron cyclotron resonance plasma etching with low radio-frequency substrate bias *Appl. Phys. Lett.* **68** 316
- [44] Maruyama T, Fujiwara N, Ogino S and Miyatake H 1998 Reduction of charge build-up with pulse-modulated bias in pulsed electron cyclotron resonance plasma *Japan. J. Appl. Phys.* **37** 2306

- [45] Midha V and Economou D J 2000 Spatiotemporal evolution of a pulsed chlorine discharge *Plasma Sources Sci. Technol.* **9** 256
- [46] Hebner G A and Fleddermann C B 1997 Characterization of pulse-modulated inductively coupled plasmas in argon and chlorine *J. Appl. Phys.* **82** 2814
- [47] Malyshev M V, Donnelly V M, Colonell J I and Samukawa S 1999 Dynamics of pulsed-power chlorine plasmas *J. Appl. Phys.* **86** 4813
- [48] Ahn T H, Nakamura K and Sugai H 1996 Negative ion measurements and etching in a pulsed power inductively coupled plasma in chlorine *Plasma Sources Sci. Technol.* **5** 139
- [49] Economou D 2007 Fundamentals and applications of ion-ion plasmas *Appl. Surf. Sci.* **253** 6672
- [50] Rogoff G L 1985 Ambipolar diffusion coefficients for discharges in attaching gases *J. Phys. D: Appl. Phys.* **18** 1533
- [51] Malyshev M V and Donnelly V M 2000 Dynamics of inductively-coupled pulsed chlorine plasmas in the presence of continuous substrate bias *Plasma Sources Sci. Technol.* **9** 353
- [52] Ashida S and Lieberman M A 1997 Spatially averaged (global) model of time modulated high density chlorine plasmas *Japan. J. Appl. Phys.* **36** 854
- [53] Meyyappan M 1997 Modeling of pulsed-power SF<sub>6</sub> plasma *Japan. J. Appl. Phys.* **36** 4820
- [54] Meyyappan M 1996 Analysis of pulse-time modulated high density plasmas *J. Vac. Sci. Technol. A* **14** 2122
- [55] Kaganovich I D and Tsendin L D 1993 Formation of discontinuities in multistage evolution associated with diffusion of a multicomponent weakly ionized hot-electron plasma *Plasma Phys. Rep.* **19** 645
- [56] Kaganovich I D, Ramamurthi B N and Economou D J 2001 Spatiotemporal dynamics of charged species in the afterglow of plasmas containing negative ions *Phys. Rev. E* **64** 036402
- [57] Kaganovich I D, Economou D J, Ramamurthi B N and Midha V 2000 Negative ion density fronts during ignition and extinction of plasmas in electronegative gases *Phys. Rev. Lett.* **84** 1918
- [58] Brihoum M, Cunge G, Darnon M, Gahan D, Joubert O and Braithwaite N St J 2013 Ion flux and ion distribution function measurements in synchronously pulsed inductively coupled plasmas *J. Vac. Sci. Technol. A* **31** 020604
- [59] Lichtenberg A J, Vahedi V, Lieberman M A and Rognlien T 1994 Modeling electronegative plasma discharges *J. Appl. Phys.* **75** 2339
- [60] Thorsteinsson E G and Gudmundsson J T 2010 A global (volume-averaged) model of a Cl<sub>2</sub>/Ar discharge: II. Pulsed power modulation *J. Phys. D: Appl. Phys.* **43** 115202
- [61] D Smith, Dean A G and Adams N G 1974 Space charge fields in afterglow plasmas *J. Phys. D: Appl. Phys.* **7** 1944
- [62] Gutsev S A, Kudryavtsev A A and Romanenko V A 1995 Formation of an ion-ion plasma as a result of electron runaway in the pauses of pulsed discharge in oxygen *Tech. Phys.* **40** 1131
- [63] Kudryavtsev A A and Tsendin L D 2000 On the possibility of negative ion concentration growth between pulses of discharge current in oxygen *Tech. Phys. Lett.* **26** 582
- [64] Belostotsky S G, Economou D J, Lopaev D V and Rakhimova T V 2005 Negative ion destruction by O(<sup>3</sup>P) atoms and O<sub>2</sub>(<sup>1</sup>Δ<sub>g</sub>) molecules in an oxygen plasma *Plasma Sources Sci. Technol.* **14** 532
- [65] Hansen S G, Luckman G and Colson S D 1988 Measurements of F\*, CF and CF<sub>2</sub> formation and decay in pulsed fluorocarbon discharges *Appl. Phys. Lett.* **53** 1588
- [66] Takahashi K, Hori M and Goto T 1993 Control of fluorocarbon radicals by on-off modulated electron cyclotron resonance plasma *Japan. J. Appl. Phys. Part 2* **32** L1088
- [67] Booth J P, Cunge G, Chabert P and Sadeghi N 1999 CF<sub>x</sub> radical production and loss in a CF<sub>4</sub> reactive ion etching plasma: fluorine-rich conditions *J. Appl. Phys.* **85** 3097
- [68] Cunge G and Booth J P 1999 CF<sub>2</sub> production and loss mechanisms in fluorocarbon discharges: fluorine-poor conditions and polymerization *J. Appl. Phys.* **85** 3952
- [69] Goto T and Hori M 1996 Radical behavior in fluorocarbon plasma and control of silicon oxide etching by injection of radicals *Japan. J. Appl. Phys. Part 1* **35** 6521
- [70] Vempaire D and Cunge G 2009 Probing radical kinetics in the afterglow of pulsed discharges by absorption spectroscopy with light emitting diodes: application to BCl radical *Appl. Phys. Lett.* **94** 021504
- [71] Cunge G, Vempaire D, Ramos R, Touzeau M, Joubert O, Bodard P and Sadeghi N 2010 Radical surface interactions in industrial silicon plasma etch reactors *Plasma Sources Sci. Technol.* **19** 034017
- [72] Kono A, Haverlag M, Kroesen G M W and de Hoog F J 1991 Temporal behavior of the electron and negative ion densities in a pulsed radio frequency CF<sub>4</sub> plasma *J. Appl. Phys.* **70** 2930
- [73] Bodard P, Brihoum M, Cunge G, Joubert O and Sadeghi N 2011 Analysis of pulsed high-density HBr and Cl<sub>2</sub> plasmas: impact of the pulsing parameters on the radical densities *J. Appl. Phys.* **110** 113302
- [74] Hargis P J *et al* 1994 The gaseous electronics conference radio-frequency reference cell: a defined parallel-plate radio-frequency system for experimental and theoretical studies of plasma-processing discharges *Rev. Sci. Instrum.* **65** 140
- [75] Miller P A, Hebner G A, Pochan P D, Greenberg K E and Aragon B P 1995 An inductively coupled plasma source for the gaseous electronics conference rf reference cell *J. Res. Natl. Inst. Stand. Technol.* **100** 427
- [76] Ramamurthi B and Economou D J 2002 Two-dimensional pulsed-plasma simulation of a chlorine discharge *J. Vac. Sci. Technol. A* **20** 467
- [77] Agarwal A, Stout P J, Banna S, Rauf S and Collins K 2011 Recouping etch rates in pulsed inductively coupled plasmas *J. Vac. Sci. Technol. A* **29** 011017
- [78] Wagner J A and Katsch H-M 2006 Negative oxygen ions in a pulsed RF-discharge with inductive coupling in mixtures of noble gases and oxygen *Plasma Sources Sci. Technol.* **15** 156
- [79] Hayashi D and Kadota K 1998 Measurements of negative ion density in high-density oxygen plasmas by probe-assisted laser photodetachment *J. Appl. Phys.* **83** 697
- [80] Panda S, Economou D J and Meyyappan M 2000 Effect of metastable oxygen molecules in high-density power modulated oxygen discharges *J. Appl. Phys.* **87** 8323
- [81] Ashida S, Lee C and Lieberman M A 1995 Spatially averaged (global) model of time modulated high density argon plasmas *J. Vac. Sci. Technol. A* **13** 2498
- [82] Yokozawa A, Ohtake H and Samukawa S 1996 Simulation of pulse time-modulated bulk plasma in Cl<sub>2</sub> *Japan. J. Appl. Phys.* **35** 2433
- [83] Lee C, Graves D B, Lieberman M A and Hess D W 1994 Global model of plasma chemistry in a high density oxygen discharge *J. Electrochem. Soc.* **141** 1546
- [84] Hopkins M B and Graham W G 1991 Time-resolved electron energy distribution function measurements in a pulsed magnetic multipole hydrogen discharge *J. Appl. Phys.* **69** 3461
- [85] Béchu S, Soum-Glaude A, Bès A, Lacoste A, Svarnas P, Aleiferis S, Ivanov A A Jr and Bacal M 2013 Multi-dipolar

- microwave plasmas and their application to negative ion production *Phys. Plasmas* **20** 101601
- [86] Monahan D D and Turner M M 2008 Global models of electronegative discharges: critical evaluation and practical recommendations *Plasma Sources Sci. Technol.* **17** 045003
- [87] Samukawa S, Sakamoto K and Ichiki K 2001 Generating high-efficiency neutral beams by using negative ions in an inductively coupled plasma source *Japan. J. Appl. Phys. Part 2* **40** L779
- [88] Panda S, Economou D J and Chen L 2001 Anisotropic etching of polymer films by high energy ( $\sim 100$ s of eV) oxygen atom neutral beams *J. Vac. Sci. Technol. A* **19** 398
- [89] Kanakasabapathy S K, Overzet L J, Midha V and Economou D J 2001 Alternating fluxes of positive and negative ions from an ion–ion plasma *Appl. Phys. Lett.* **78** 22
- [90] Kaganovich I, Ramamurthi D B and Economou D J 2000 Self-trapping of negative ions due to electron detachment in the afterglow of electronegative gas plasmas *Appl. Phys. Lett.* **76** 2844
- [91] Overzet L J, Smith B A, Kleber J and Kanakasabapathy S K 1997 Negative ion extraction from pulsed discharges *Japan. J. Appl. Phys.* **36** 2443
- [92] Maeshige K, Washio G, Yagisawa T and Makabe T 2002 Functional design of a pulsed two-frequency capacitively coupled plasma in  $\text{CF}_4/\text{Ar}$  for  $\text{SiO}_2$  etching *J. Appl. Phys.* **91** 9494
- [93] Yagisawa T and Makabe T 2003 Temporal velocity distribution of positive and negative ions incident on a wafer in a pulsed two-frequency capacitively coupled plasma in  $\text{CF}_4/\text{Ar}$  for  $\text{SiO}_2$  etching *IEEE Trans. Plasma Sci.* **31** 521
- [94] Agarwal A, Stout P J, Banna S, Rauf S, Tokashiki K, Lee J-Y and Collins K 2009 Effect of simultaneous source and bias pulsing in inductively coupled plasma etching *J. Appl. Phys.* **106** 103305
- [95] Subramonium P and Kushner M J 2004 Extraction of negative ions from pulsed electronegative inductively coupled plasmas having a radio frequency substrate bias *J. Vac. Sci. Technol. A* **22** 534
- [96] Riemann K-U 2003 Kinetic analysis of the collisional plasma–sheath transition *J. Phys. D: Appl. Phys.* **36** 2811
- [97] Kortshagen U and Zethoff M 1995 Ion energy distribution functions in a planar inductively coupled RF discharge *Plasma Sources Sci. Technol.* **4** 541
- [98] Aydil E S, Quiniou B O M, Lee J T C, Gregus J A and Gottscho R A 1998 Incidence angle distributions of ions bombarding grounded surfaces in high density plasma reactors *Mater. Sci. Semicond. Process.* **1** 75
- [99] Diomede P, Longo S, Economou D J and Capitelli M 2012 Hybrid simulation of a dc-enhanced radio-frequency capacitive discharge in hydrogen *J. Phys. D: Appl. Phys.* **45** 175204
- [100] Nam S K, Economou D J and Donnelly V M 2007 Particle-in-cell simulation of ion beam extraction from a pulsed plasma through a grid *Plasma Sources Sci. Technol.* **16** 90
- [101] Smith B A and Overzet L J 1995 Time-resolved energy distributions of  $\text{F}^-$  from pulsed radio frequency discharges *J. Appl. Phys.* **78** 5195
- [102] Coburn J W and Kay E 1972 Positive-ion bombardment of substrates in rf diode glow discharge sputtering *J. Appl. Phys.* **43** 4965
- [103] Diomede P, Donnelly V M and Economou D J 2011 Particle-in-cell simulation of ion energy distributions on an electrode by applying tailored bias waveforms in the afterglow of a pulsed plasma *J. Appl. Phys.* **109** 083302
- [104] Diomede P, Kim D and Economou D J 2013 Particle-in-cell simulation of electron and ion energy distributions in dc/RF hybrid capacitively-coupled plasmas *AICHE J.* **59** 3214
- [105] Godyak V A, Piejak R B and Alexandrovich B M 1992 Measurement of electron energy distribution in low-pressure RF discharges *Plasma Sources Sci. Technol.* **1** 36
- [106] Sugai H, Ghanashev I, Hosokawa M, Mizuno K, Nakamura K, Toyoda H and Yamauch K 2001 Electron energy distribution functions and the influence on fluorocarbon plasma chemistry *Plasma Sources Sci. Technol.* **10** 378
- [107] Song S-H and Kushner M J 2012 Control of electron energy distributions and plasma characteristics of dual frequency, pulsed capacitively-coupled plasmas sustained in Ar and  $\text{Ar}/\text{CF}_4/\text{O}_2$  *Plasma Sources Sci. Technol.* **21** 055028
- [108] Sun J, Li X, Sang C, Jiang W, Zhang P and Wang D 2010 Particle-in-cell simulation of hydrogen discharge driven by combined radio frequency and pulse sources *Phys. Plasmas* **17** 103505
- [109] Gozadinos G, Vender D, Turner M M and Lieberman M A 2001 Collisionless electron heating by capacitive radio-frequency plasma sheaths *Plasma Sources Sci. Technol.* **10** 117
- [110] Boswell R W and Henry D 1985 Pulsed high rate plasma etching with variable  $\text{Si}/\text{SiO}_2$  selectivity and variable Si etch profiles *Appl. Phys. Lett.* **47** 1095
- [111] Samukawa S and Furuoya S 1993 Time-modulated electron cyclotron resonance discharge for controlling generation of reactive species *Appl. Phys. Lett.* **63** 2044
- [112] Petit-Etienne C, Darnon M, Bodart P, Fouchier M, Cunge G, Pargon E, Vallier L and Joubert O 2013 Atomic scale silicon etching control using pulsed plasma *J. Vac. Sci. Technol. B* **31** 011201
- [113] Athavale S and Economou D J 1996 Realization of atomic layer etching (ALET) of silicon *J. Vac. Sci. Technol. B* **14** 3702
- [114] Athavale S D and Economou D J 1995 Molecular dynamics simulation of atomic layer etching (ALET) of silicon *J. Vac. Sci. Technol. A* **13** 966
- [115] Donnelly V M and Economou D J 2009 Atomic layer etching with pulsed plasmas *US and International Patents* Provisional patent application No. 61/286, 572
- [116] Hwang G S and Giapis K P 1998 Mechanism of charging reduction in pulsed plasma etching *Japan J. Appl. Phys.* **37** 2291
- [117] Ishikawa Y, Ichihashi Y, Yamasaki S and Samukawa S 2008 UV photon-induced defect and its control in plasma etching processes *J. Appl. Phys.* **104** 063306
- [118] Ono K and Tuda M 2000 Dynamics of plasma–surface interactions and feature profile evolution during pulsed plasma etching *Thin Solid Films* **374** 208
- [119] Schaepekens M, Oehrlein G S and Cook J M 2000 Effects of radio frequency bias frequency and radio frequency bias pulsing on  $\text{SiO}_2$  feature etching in inductively coupled fluorocarbon plasma *J. Vac. Sci. Technol. B* **18** 856
- [120] Raballand V, Cartry G and Cardinaud C 2007 Porous  $\text{SiOCH}$ ,  $\text{SiCH}$  and  $\text{SiO}_2$  etching in high density fluorocarbon plasma with a pulsed bias *Plasma Process. Polym.* **4** 563
- [121] Banna S *et al* 2009 Inductively coupled pulsed plasmas in the presence of synchronous pulsed substrate bias for robust, reliable, fine conductor etching *IEEE Trans. Plasma Sci.* **37** 1730
- [122] Cicala G 2012 Deposition of carbon based materials by continuous and pulsed discharges *Surf. Eng.* **28** 141
- [123] Winder E J and Gleason K K 2000 Growth and characterization of fluorocarbon thin films grown from

- trifluoromethane ( $\text{CHF}_3$ ) using pulsed-plasma enhanced CVD *J. Appl. Polym. Sci.* **78** 842
- [124] Pedersen H, Larsson P, Aijaz A, Jensen J and Lundin D 2012 A novel high-power pulse PECVD method *Surf. Coat. Technol.* **206** 4562
- [125] Agarwal A and Kushner M J 2009 Plasma atomic layer etching using conventional plasma equipment *J. Vac. Sci. Technol. A* **27** 37
- [126] Park S-D, Min K-S, Yoon B-Y, Lee D-H and Yeom G-Y 2005 Precise depth control of silicon etching using chlorine atomic layer etching *Japan. J. Appl. Phys.* **44** 389
- [127] Park S D, Oh C K, Lee D H and Yeom G Y 2005 Surface roughness variation during Si atomic layer etching by chlorine adsorption followed by an Ar neutral beam irradiation *Electrochem. Solid State Lett.* **8** C177
- [128] Metzler D, Bruce R L, Engelmann S, Joseph E A and Oehrlein G S 2014 Fluorocarbon assisted atomic layer etching of  $\text{SiO}_2$  using cyclic Ar/ $\text{C}_4\text{F}_8$  plasma *J. Vac. Sci. Technol. A* **32** 020603
- [129] Economou D J 2008 Fast (10s–100s eV) neutral beams for materials processing *J. Phys. D: Appl. Phys.* **41** 024001
- [130] Ranjan A, Donnelly V M and Economou D J 2006 Energy distribution and flux of fast neutrals and residual ions extracted from a neutral beam source *J. Vac. Sci. Technol. A* **24** 1839
- [131] Todorow V, Holland J and Gani N 2004 *US Patent* 6818562  
Chen J-Y, Holland J P, Sato A H and Todorow V N 2002 *US Patent* 6472822  
Banna S, Todorow V and Ramaswamy K 2009 *US Patent* 0284156 A1
- [132] Liu L, Sridhar S, Zhu W, Donnelly V M and Economou D J *unpublished*